

AN ABSTRACT OF THE THESIS OF

Christina D. Knierim for the degree of Honors Baccalaureate of Science in Civil Engineering presented on November 26, 2014. Title: Geotechnical Characterization and Drained Shear Strength of a Limestone Aggregate

Abstract approved:

Armin Stuedlein

Aggregate piers are a method of ground improvement used to increase the strength and bearing capacity of the native geological soils for the support of new civil infrastructure. The understanding of the bearing failure mechanism of aggregate piers remains largely unstudied. The effects of design variables in the failure mechanisms are not fully understood. This study determined the geotechnical characterization and drained shear strength of a limestone aggregate of specific gradation commonly used for the construction of aggregate piers. The index properties and drained shear strength parameters were found using consolidated drained, axisymmetric triaxial testing. Five confining stresses were chosen to model the stresses an aggregate pier would be subjected to in situ and at a given depth. Dilation occurred at most of the confining stresses but decreased in magnitude with increased confining stresses until no dilative behavior occurred at the highest confining stress. The specimens all demonstrated strain softening behavior without a distinctive peak and a gradual decrease in principal stress difference after failure. The friction angle did not vary significantly within a large range of relative densities. Small differences were observed between the peak and residual friction angles, with the difference decreasing at higher confining pressures.

Key words: Triaxial test, Aggregate, Geotechnical, Void Ratio, Friction Angle

Corresponding e-mail address: knierimc@onid.oregonstate.edu

Geotechnical Characterization and Drained Shear Strength of a Limestone

Aggregate

By

Christina D. Knierim

A PROJECT

submitted to

Oregon State University

University Honors College

In partial fulfillment of the
requirements for the
degree of

Honors Baccalaureate of Science in Civil Engineering (Honors Scholar)

Presented November 26, 2014

Commencement June 2015

Honors Baccalaureate of Science in Civil Engineering project of Christina D. Knierim
presented on November 26, 2014.

APPROVED:

Armin Stuedlein, Ph.D., P.E.
Mentor, representing Civil and Construction Engineering

Chris Bell, Ph.D., P.E.
Committee Member, representing Civil and Construction Engineering

Jason Ideker, Ph.D.
Committee Member, representing Civil and Construction Engineering

Head, School of Civil and Construction Engineering

Dean, University Honors College

I understand that my project will become part of the permanent collection of Oregon State University, University Honors College. My signature below authorized release of my project to any reader upon request.

Christina D. Knierim, Author

Acknowledgments

First and foremost I would like to thank my thesis mentor, Armin Stuedlein, for the dedication and patience he has shown throughout the research and writing process. I would also like to thank my research partner Chris Newton for all the hard work in the lab, and James Walters for his instruction on how to operate the triaxial equipment. To Chris Bell and Jason Ideker for finding the time to serve on my committee on short notice, your assistance is much appreciated.

And a huge thank you to all my friends and family who have supported me, pushed me, and been patient with me through the whole process. I couldn't have done it without all of you behind me.

And lastly, I would like to thank my wonderful fiancé, Jake, for making sure I spent time on my thesis, encouraging me when I got stressed, and for loving me. Always and forever.

Table of Contents

| | |
|--|----|
| 1.0 Introduction | 1 |
| 2.0 Literature Review | 3 |
| 2.1 Aggregate Pier Ground Improvement | 3 |
| 2.1.1 General | 3 |
| 2.1.2 Construction Methods..... | 4 |
| 2.2 Triaxial Strength Response of a typical aggregate | 6 |
| 2.2.1 Mohr-Coulomb Failure Criterion and Shear Strength Parameters | 7 |
| 2.2.2 Geotechnical Characterization of Aggregate | 8 |
| 2.3 General Behavior of an Aggregate Pier in Clayey Soil | 13 |
| 2.4 Factors Affecting Bearing Capacity | 15 |
| 2.5 Summary | 16 |
| 3.0 Research Objectives and Program | 18 |
| 3.1 Research Objectives | 18 |
| 3.2 Research Program | 18 |
| 4.0 Triaxial Test Program | 20 |
| 4.1 Equipment | 20 |
| 4.2 Test Methodology | 21 |
| 4.2.1 Sieving Aggregates for Specimen Preparation..... | 21 |
| 4.2.2 Specimen Preparation | 23 |
| 4.2.3 Mounting the Specimen..... | 24 |
| 4.2.4 Specimen Shearing Procedures | 27 |
| 5.0 Results | 29 |
| 5.1 Grain Size Distribution | 29 |
| 5.2 Minimum and Maximum Void Ratio and Compaction Characteristics 30 | |
| 5.3 Constitutive Properties of the Aggregate | 33 |
| 5.3.1 Experimental Stress-Strain Response | 35 |
| 5.3.2 Volumetric Strain- Axial Strain Response | 37 |
| 5.3.3 Hyperbolic Model Parameters from Duncan et al. (1980) | 38 |
| 5.3.4 Peak and Residual Friction Angles..... | 43 |
| 5.4 Stress-strain and Volumetric Strain Response of the Aggregate in Comparison to Duncan et al. (2007) | 45 |
| 5.5 Summary of Results | 50 |

Table of Contents (continued)

| | |
|--|-----------|
| 6.0 Summary, Conclusions, and Suggestions for Further Study | 52 |
| 6.1 Summary of Research Performed..... | 52 |
| 6.2 Conclusions | 52 |
| 6.3 Suggestions for Further Study | 54 |
| References | 55 |
| Appendix A: Stress-Strain and Volumetric Strain Curves for Individual Tests | 57 |
| Appendix B: Data used for Hyperbolic Stress-Strain Curves | 62 |

List of Figures

| | |
|--|----|
| Figure 2.1 Vibro Pier™ (Hayward Baker 2012a)..... | 5 |
| Figure 2.2 Vibro-replacement using the dry installation method (Hayward Baker 2012b). | 6 |
| Figure 2.3: Schematic of a typical triaxial apparatus (after Holtz et al. 2011) | 7 |
| Figure 2.3: Mohr-Coulomb envelope for low density #57 aggregate (after Duncan et al. 2007) | 11 |
| Figure 2.4: Mohr-Coulomb envelope for high density #57 aggregate (after Duncan et al. 2007) | 11 |
| Figure 2.5: Confining pressure vs Friction angle for #57 aggregate (after Duncan et al. 2007) | 12 |
| Figure 2.6 Stresses on a single, isolated aggregate pier (after Stuedlein and Holtz 2013) | 15 |
| Figure 4.1 Triaxial station..... | 21 |
| Figure 4.2 Aggregate used in this study..... | 22 |
| Figure 4.3 Compacted specimen on custom compaction base..... | 24 |
| Figure 4.4 Transfer of specimen from compaction base to triaxial base | 25 |
| Figure 4.5 Specimen with top platen, drainage lines and under vacuum..... | 26 |
| Figure 4.6 Specimen during CO ₂ flush (from Walters) | 27 |
| Figure 5.1 Grain Size Distribution | 30 |
| Figure 5.2 Modified Proctor compaction curve (from Newton 2014)..... | 33 |
| Figure 5.3 Principal stress difference, q , versus axial strain, ϵ_1 | 36 |
| Figure 5.4 Axial Strain at failure vs Confining Pressure | 36 |
| Figure 5.5 Young's Modulus vs Confining Pressure | 37 |
| Figure 5.6 Volumetric Strain, ϵ_v , versus axial strain, ϵ_1 | 38 |
| Figure 5.7 Hyperbolic stress-strain curve compared to actual stress-strain curve for 21 kPa confining stress | 41 |
| Figure 5.8 Hyperbolic stress-strain curve compared to actual stress-strain curve for 48 kPa confining stress | 41 |
| Figure 5.9 Hyperbolic stress-strain curve compared to actual stress-strain curve for 101 kPa confining stress | 42 |
| Figure 5.10 Hyperbolic stress-strain curve compared to actual stress-strain curve for 257 kPa confining stress | 42 |

List of Figures (continued)

| | |
|---|----|
| Figure 5.11 Hyperbolic stress-strain curve compared to actual stress-strain curve for 375 kPa confining stress | 43 |
| Figure 5.12 Peak and Residual Friction Angles versus Confining Stress..... | 44 |
| Figure 5.13 Aggregate gradation used in this study as compared to #57 limestone gradation from Duncan et al. (2007)..... | 45 |
| Figure 5.14 Principal stress difference versus axial strain for 21 kPa confining pressure from this study compared to 27 kPa confining pressure from Duncan et al. (2007) | 46 |
| Figure 5.15 Principal stress difference versus axial strain for 48 kPa confining pressure from this study compared to 56 kPa confining pressure from Duncan et al. (2007) | 47 |
| Figure 5.16 Principal stress difference versus axial strain for 250 kPa confining pressure from this study compared to 209 kPa confining pressure from Duncan et al. (2007) | 47 |
| Figure 5.17 Volumetric strain versus axial strain for 21 kPa confining pressure from this study compared to 27 kPa confining pressure from Duncan et al. (2007)..... | 48 |
| Figure 5.18 Volumetric strain versus axial strain for 48 kPa confining pressure from this study compared to 56 kPa confining pressure from Duncan et al. (2007)..... | 48 |
| Figure 5.19 Volumetric strain versus axial strain for 250 kPa confining pressure from this study compared to 209 kPa confining pressure from Duncan et al. (2007)..... | 49 |
| Figure 5.20 Friction angle versus confining stress for the aggregate used in this study and the #57 limestone from Duncan et al. (2007) | 50 |
| Figure A.1 Principal stress difference versus axial strain for specimen sheared at 21 kPa effective confining stress, dashed line indicates strain at failure..... | 57 |
| Figure A.2 Volumetric strain versus axial strain for specimen sheared at 21 kPa effective confining stress, dashed line indicates strain at failure..... | 58 |
| Figure A.3 Principal stress difference versus axial strain for specimen sheared at 48 kPa effective confining stress, dashed line indicates strain at failure..... | 58 |
| Figure A.4 Volumetric strain versus axial strain for specimen sheared at 48 kPa effective confining stress, dashed line indicates strain at failure..... | 59 |
| Figure A.5 Principal stress difference versus axial strain for specimen sheared at 101 kPa effective confining stress, dashed line indicates strain at failure..... | 59 |

List of Figures (continued)

| | |
|--|----|
| Figure A.6 Volumetric strain versus axial strain for specimen sheared at 101 kPa effective confining stress, dashed line indicates strain at failure | 60 |
| Figure A.7 Principal stress difference versus axial strain for specimen sheared at 257 kPa effective confining stress, dashed line indicates strain at failure | 60 |
| Figure A.8 Volumetric strain versus axial strain for specimen sheared at 257 kPa effective confining stress, dashed line indicates strain at failure | 61 |
| Figure A.9 Principal stress difference versus axial strain for specimen sheared at 375 kPa effective confining stress, dashed line indicates strain at failure | 61 |
| Figure A.10 Volumetric strain versus axial strain for specimen sheared at 375 kPa effective confining stress, dashed line indicates strain at failure | 62 |

List of Tables

| | |
|---|----|
| Table 2.1: Maximum dry densities (after Duncan et al. 2007) | 9 |
| Table 2.2: Summary of results for #57 limestone aggregate (after Duncan et al. 2007) .. | 13 |
| Table 4.1 Test gradation..... | 22 |
| Table 5.1 Maximum Void Ratio Trials..... | 31 |
| Table 5.2 Effective Confining Stress and Pre and Post Consolidation Relative Density . | 34 |
| Table B.1 Data used for Hyperbolic Stress-Strain Curves..... | 62 |

Geotechnical Characterization and Drained Shear Strength of a Limestone Aggregate

1.0 Introduction

The demand for new civil infrastructure (e.g., buildings, roads, and bridges) in locations that pose construction difficulties have led to an increased need for innovative ground improvement technologies. Increasingly, the native geological soil available for development is incapable of supporting the loads imposed by new structures. When these soils are built upon without any additional engineering, the soils can settle and cause the structure to experience significant distress and in extreme cases, fail. In some cases, the soils may appear to be strong enough, but can later fail if liquefaction occurs during an earthquake.

In order to address this problem, geotechnical engineers use techniques to improve the native soil and increase the strength and bearing capacity of structure foundations. Many methods have been invented and employed for the improvement of soil. Aggregate pier ground improvement is one such method for increasing the load-bearing capacity of the soil. Often the upper layers of soil are weak, but a stronger layer lies deeper within the subsurface. Aggregate piers assist in transferring the loads through the weaker soils and into the stronger layers, as described in the subsequent literature review chapter.

This study used a limestone aggregate of specific gradation commonly used for the construction of aggregate piers. The research resulted in the determination of the geotechnical index characteristics including the determination of the minimum and

maximum void ratio, optimum and dry unit weight, modified Proctor compaction characteristics, and the drained shear strength of this aggregate at a range of confining stresses which represented the range of possible stresses over the course of the service life of an aggregate pier. The characterization of the engineering properties of this construction material will be applied to ongoing research into aggregate pier ground improvement. For example, this research provided a baseline for a study on the effect of cementation of the aggregate on the increase in the bearing capacity of aggregate piers.

Chapter 2 of this thesis provides a review of the relevant literature on aggregate pier ground improvement. Chapter 3 summarizes the research objective and program developed to achieve the research objectives. Chapter 4 describes the experimental program in detail, and is followed by the description of results in Chapter 5. Chapter 6 summarizes the findings developed over the course of this research and is followed by the references and appendices.

2.0 Literature Review

Aggregate piers, also known as stone columns, are one kind of ground improvement alternative used by engineers as a means to improve the native soil in order to support loads from new civil infrastructure. Aggregate piers assist by transferring the load through the weaker layers and into stronger layers deeper with the ground (end-bearing piers), or by spreading the load along the length of the pier (floating or frictional piers). Since aggregate piers are constructed with aggregate and don't use more expensive materials such as steel or concrete, they are an economically viable means of ground improvement when compared to alternatives such as deep foundations (e.g. drilled shafts or driven piles) or expensive stiffened mat foundations.

This chapter summarizes the construction methods, materials, and general engineering of aggregate pier ground improvement. First, two common construction methods are described. Then, geotechnical characterization and strength parameters of a typical aggregate are reviewed and are followed by a description of the behavior of an aggregate pier in clayey soil. The literature review is concluded with a brief discussion of the factors affecting bearing capacity.

2.1 Aggregate Pier Ground Improvement

2.1.1 General

Aggregate piers are columns of crushed rock aggregate that is constructed within the soil that acts as a means to transfer or spread the gravitational and live loads from a structure. As mentioned above, there are two main types of aggregate piers: end-

bearing piers and frictional piers. End-bearing piers are used when a stronger strata is located below the weaker one. In this case, the pier is built to a depth within the stronger soil and the load is transferred through the weak soil and into the stronger which is capable of bearing the loads without failure. Frictional piers are used when there is no stronger soil deposit easily or economically accessible. In this case, the piers transfer load to the soil along the length of the pier through side-friction, rather than in a concentrated load. In both cases, aggregate piers are able to increase the bearing capacity of the native soils and decrease total and differential settlement. They also reduce the time needed for the consolidation of fine-grained soil, and lower the risk of liquefaction in the case of seismic events.

2.1.2 Construction Methods

Although there are a number of methods for aggregate pier construction, this review will focus on two of the most common methods used with coarse-grained aggregate in the United States: vibropiers and vibro-replacement.

Vibropiers are constructed by pre-drilling a shaft before construction. Aggregate is added to the shaft in lifts and compacted by a vibrator lowered into the shaft by a crane, as shown in Figure 2.1. The vibrator typically is raised and lowered a few times for each lift in order to assure high compaction or densification of the aggregate. The vibration densifies the aggregate and forces it into the surrounding soil. Because these shafts must be pre-drilled, they are typically used for shorter piers and/or floating piers.

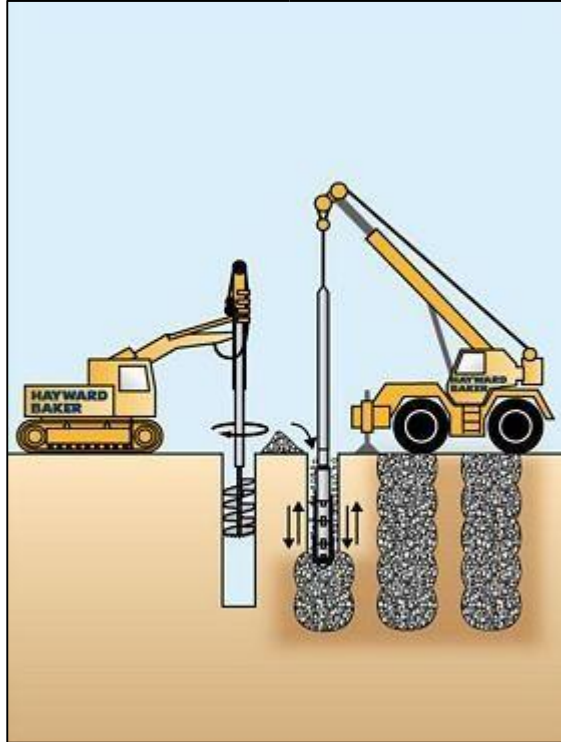


Figure 2.1 Vibro Pier™ (Hayward Baker 2012a).

Vibro-replacement piers, also known as stone columns, are constructed through either the ‘dry’ bottom feed process or the ‘wet’ top feed process (Hayward Baker 2012b). In the dry process, the vibrator is forced into the soil using only its own weight and vibration. Then the aggregate is added into an aggregate delivery tremie pipe attached to the vibrator, as seen in Figure 2.2. Similar to the vibropiers, the aggregate is introduced in lifts and compacted by raising and lowering the vibrator. The wet method is employed when additional force is necessary to advance the vibrator into the ground (Hayward Baker 2012b). This method uses water jets on the tip of the vibrator to assist the vibrator in the penetration of the soil. The aggregate for this process is added from the ground level to fill the additional space around the vibrator created by the jets. Then the vibrator is raised and lowered in a similar fashion as described above to compact the aggregate.

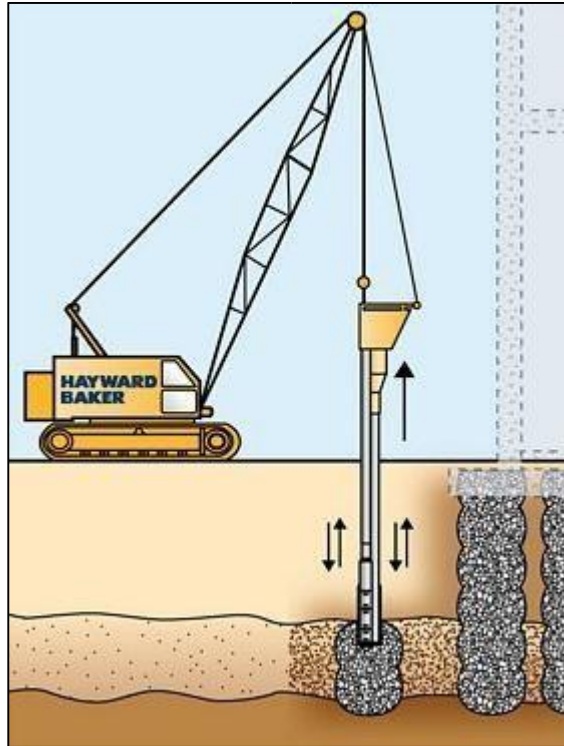


Figure 2.2 Vibro-replacement using the dry installation method (Hayward Baker 2012b).

2.2 Triaxial Strength Response of a typical aggregate

Triaxial tests are used to determine the strength parameters of a material, such as aggregate. Triaxial tests involve loading a cylindrical specimen (usually encased in a rubber membrane) into a larger cylindrical cell, filling the cell with water and then pressurizing it. This causes the stresses from all sides to be equal, and is termed isotropic consolidation. Then an axial load is applied to the top of the aggregate specimen by displacement of a loading platen. Drainage from the specimen can either be allowed or prevented depending on the situation being researched. This setup allows the specimen to fail on any plane, rather than a forced plane like a direct shear test (Holtz et al 2011). Figure 2.3 shows a typical triaxial setup. The data collected during a triaxial test can be

used in conjunction with the Mohr-Coulomb failure criterion described in the following section to determine the strength parameters of a material.

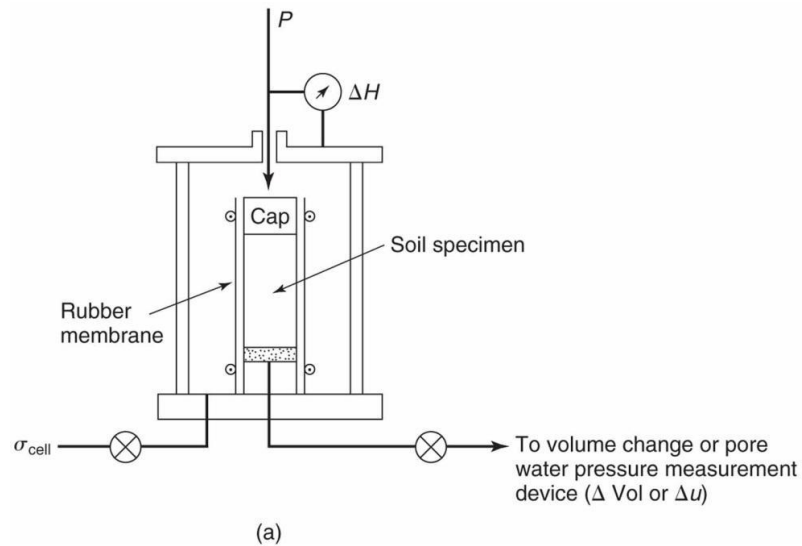


Figure 2.3: Schematic of a typical triaxial apparatus (after Holtz et al. 2011)

2.2.1 Mohr-Coulomb Failure Criterion and Shear Strength Parameters

In geotechnical engineering, the strength of a soil is equal to the maximum shear stress a material can produce. In practice, civil engineers define ‘failure’ as the stress magnitudes for which a material deforms beyond an acceptable level. The Mohr circle of stress is a graphical representation of the stress state of a material, consisting of normal stress, σ , components and shear stress, τ , components. The relationships between these components can be represented using a circle. The circle represents the stresses of a particular material at equilibrium, and references double angle trigonometry to maintain geometrical correspondence of stresses. This graph can be used to find the stresses acting on a plane of any orientation. Principal normal stresses are the stresses on a plane with no shear stress acting on it, and can be used to infer strength characteristics in a convenient

manner. These stresses are designated the primary, intermediate, and minor principal stresses (σ_1 , σ_2 , and σ_3 , respectively).

Mohr hypothesized that materials fail in shear as a function of the normal stress. This function is referred to as the Mohr failure envelope- a slightly curved line. When plotted, any Mohr circle that plots entirely below this envelope is stable and will not fail. Failure occurs when the circle is tangent to the envelope. Coulomb found that the shear strength may be represented linearly over a short range of normal stresses using two components: the angle of internal friction, ϕ , which is dependent on the stress, and cohesion, c , which is a constant. The resulting linear Mohr-Coulomb failure envelope is thus given by:

$$\tau_{ff} = \sigma_{ff} \tan \phi + c \quad (2.1)$$

where τ_{ff} is the shear stress on the failure plane at failure, and σ_{ff} is the normal stress at the same point. The maximum shear stress that a material can withstand, or its shear strength, is the shear stress acting on the failure plane at failure. For this reason τ_{ff} is often replaced with s , or shear strength. ϕ and c are referred to as the Mohr-Coulomb strength parameters. For sands or gravels and other granular materials c is generally non-existent or small, and as such may be neglected.

2.2.2 Geotechnical Characterization of Aggregate

Duncan et al. (2007) reported on an aggregate strength testing program on aggregates wherein they determined the strength parameters of standard gradations 21b and #57 (VDOT 2002 and ASTM C33-02a, respectively). Since some of these aggregates are similar to the aggregate used for this research this report is summarized below, and

the test results for the #57 aggregate are compared to the results of this study in Chapter 5.

Testing was done using crushed limestone, granite, and phyllite aggregates. Limestone and granite were used for the 21b tests, and limestone and phyllite were used for the #57 tests. The 21b materials were well-graded, ranging from approximately 10% passing the #200 sieve up to 1 inch in diameter with a coefficient of uniformity of 64 for the granite and 95 for the limestone. The #57 materials were poorly-graded, ranging from 3/8 inch to 1 inch, with a coefficient of uniformity of 1.7.

Duncan et al. (2007) used standard specification ASTM D4254 (Reapproved 2006) (ASTM 2006b) to determine the minimum dry densities of each of the aggregates. The limestone aggregates had minimum dry densities between 90-92 pcf, and the granite had a minimum dry density of approximately 99 pcf. The maximum dry density was determined by the Modified Proctor Test (ASTM D1557) because the densification on the vibratory table used for the ASTM D4253 (Reapproved 2006) (ASTM 2006a) procedure failed to achieve significant densification of the aggregate and the densities determined from these tests were significantly lower than those determined by the Standard (ASTM D698) or Modified Proctor tests. The results of these tests are summarized in Table 2.1.

Table 2.1: Maximum dry densities (after Duncan et al. 2007)

| Gradation | Mineralogy | Standard Proctor Test (pcf) | Modified Proctor Test (pcf) |
|-----------|------------|--------------------------------|--------------------------------|
| #57 | Limestone | 111 | 117 |
| #57 | Phyllite | 114 | 122 |
| 21b | Limestone | 141 | 150 |
| 21b | Granite | 138 | 144 |

Specimens were compacted to either high or low density specimens. High density specimens were compacted in lifts using a Standard Proctor hammer, whereas low density specimens were compacted using minimal hand tamping. Aggregate was not reused once compacted. The specimens were loaded into a triaxial apparatus and subjected to a variety of confining pressures and axial loading.

Duncan et al. (2007) defined failure as the maximum principal stress difference observed during shearing. Most of the triaxial test specimens reached failure with strains between 3 and 7 percent. The majority of specimens demonstrated dilation after an initially compressive response. The high density #57 limestone under low confining pressure exhibited the most dilation. A high density specimen has less void space and therefore demonstrates a smaller initial compression, while the low confining pressure allows for easier movement of the particles within the specimen and thus a greater volume change.

Mohr's circles of the #57 gravels are shown below in Figures 2.3 and 2.4 for selected tests. Only the results for the #57 aggregate will be reported here because it is the most similar to the aggregate used for this study. Refer to the full report for the results of the 21b aggregate.

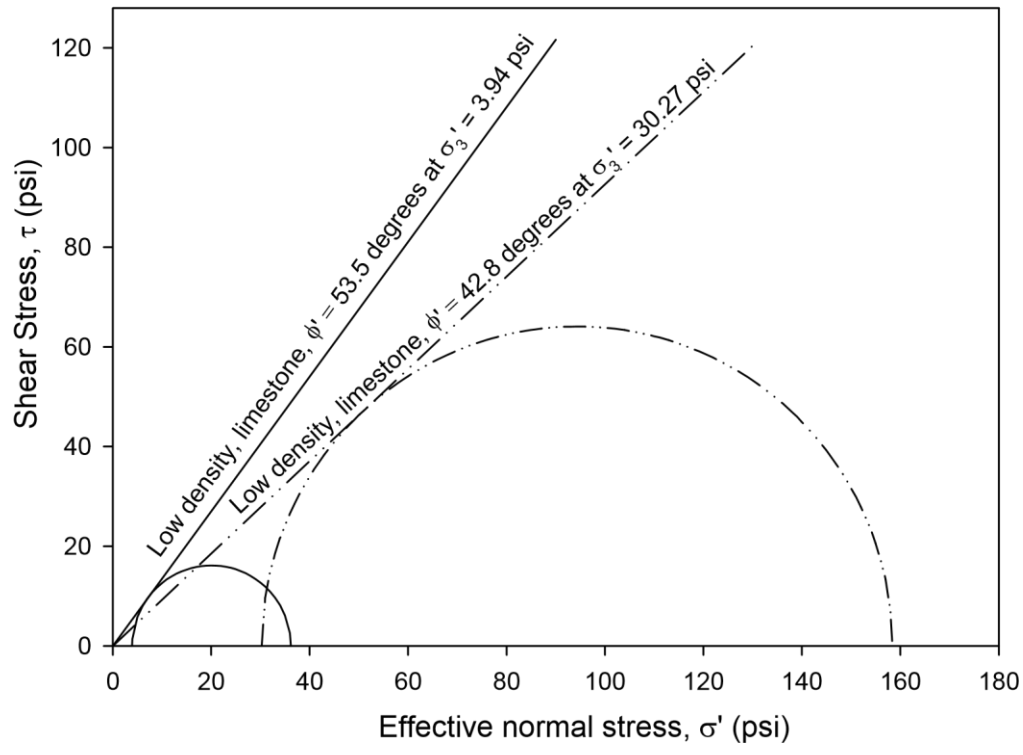


Figure 2.3: Mohr-Coulomb envelope for low density #57 aggregate (after Duncan et al. 2007)

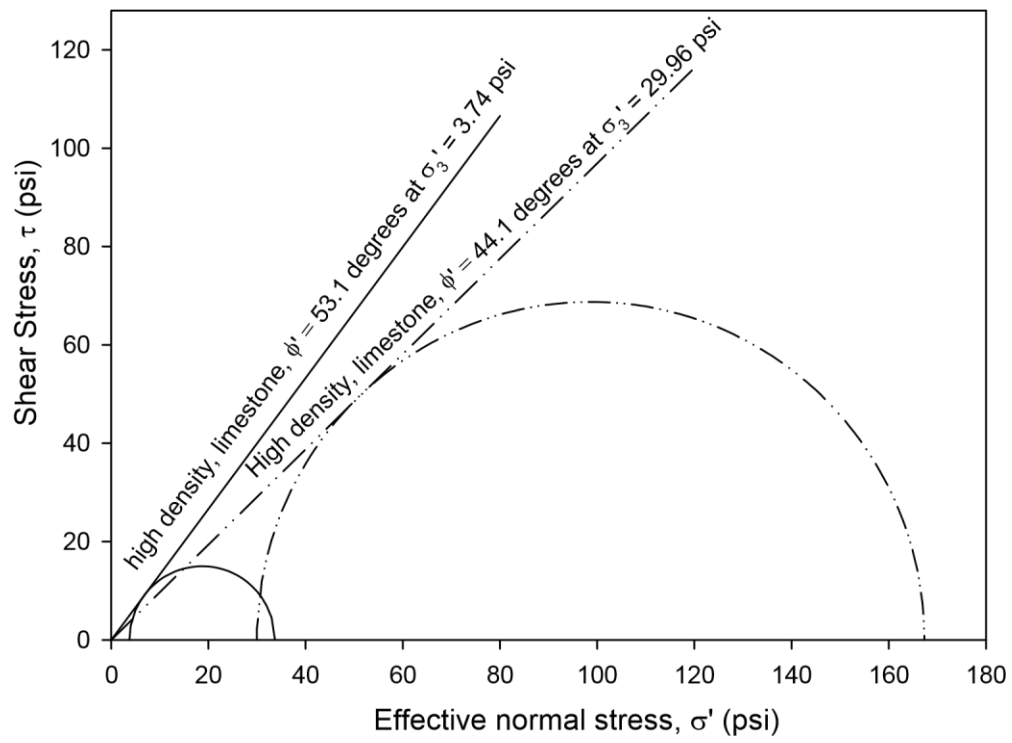


Figure 2.4: Mohr-Coulomb envelope for high density #57 aggregate (after Duncan et al. 2007)

The effective friction angles, ϕ' , were calculated for each of the tests with the assumption that the cohesion, c , was zero. When the cohesion is zero, the effective friction angle can be calculated using the following equation:

$$\phi' = \arcsin\left(\frac{q'_{\max}}{p'}\right) = \arcsin\left(\frac{(\sigma_1' - \sigma_3')_{\max}}{(\sigma_1' + \sigma_3')}\right) \quad (2.2)$$

The results showed a decrease in effective friction angle with increase of confining pressure for each of the aggregates. These variations are shown in Figure 2.5 for the #57 aggregate.

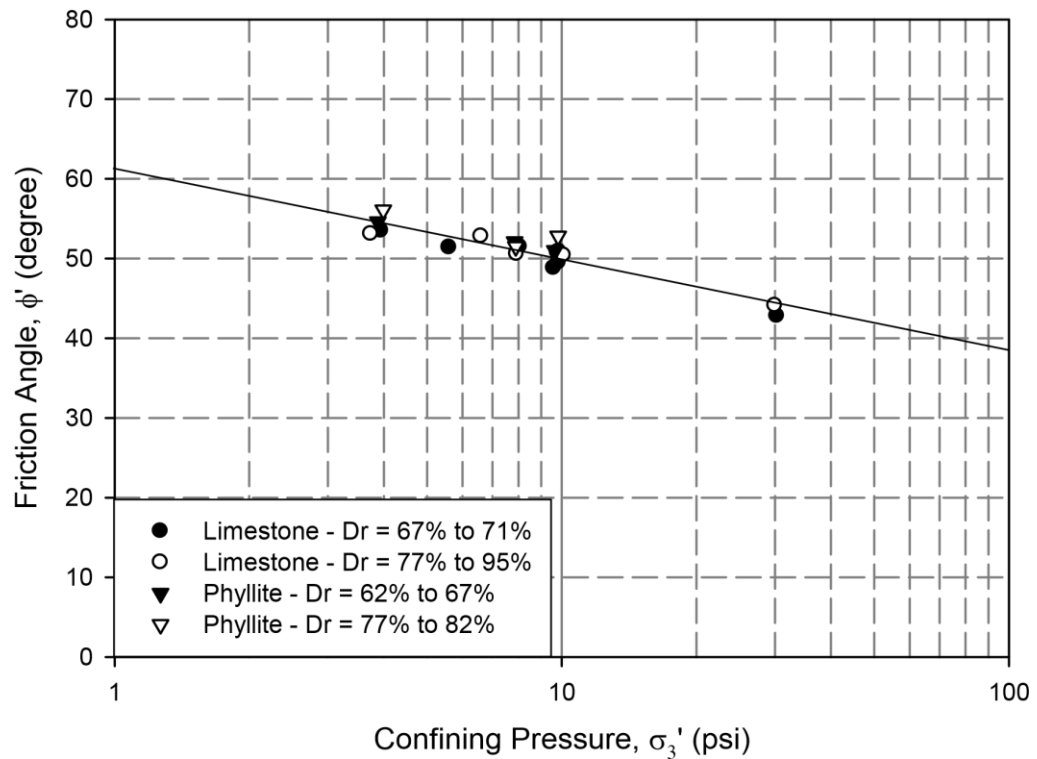


Figure 2.5: Confining pressure vs Friction angle for #57 aggregate (after Duncan et al. 2007)

It was determined from these results and the results of the 21b aggregate that this could be described as a logarithmic function,

$$\phi' = \phi'_0 - \Delta\phi' \log\left(\frac{\sigma_3'}{p_a}\right) \quad (2.3)$$

where φ'_0 is the effective friction angle for $\sigma'_3 = p_a$, σ'_3 is the effective minor principal stress, p_a is the atmospheric pressure and $\Delta\varphi'$ is the decrease in friction angle for a tenfold increase in σ'_3 . A summary of the results for the #57 limestone aggregate, which is the most similar to the aggregate used in this research is listed in Table 2. From this data it was determined that the friction angle for the #57 aggregate varies only slightly with density and is approximately 48 degrees.

Table 2.2: Summary of results for #57 limestone aggregate (after Duncan et al. 2007)

| Test no. | Relative Density (%) | σ'_3 (psi) | φ' (degrees) | φ'_0 (degrees) | $\Delta\varphi'$ (degree) |
|----------|----------------------|-------------------|----------------------|------------------------|---------------------------|
| 16 | 69 | 3.94 | 53.5 | | |
| 17 | 67 | 5.60 | 51.4 | | |
| 18 | 69 | 8.05 | 51.5 | | |
| 19 | 72 | 9.59 | 48.8 | | |
| 20 | 69 | 9.83 | 49.5 | | |
| 21 | 71 | 30.27 | 42.8 | | |
| 25 | 79 | 3.74 | 53.1 | 48.0 | 11.0 |
| 26 | 89 | 6.57 | 52.8 | | |
| 27 | 79 | 7.93 | 50.6 | | |
| 28 | 79 | 9.78 | 50.8 | | |
| 29 | 95 | 9.86 | 50.9 | | |
| 30 | 77 | 10.10 | 50.4 | | |
| 31 | 80 | 29.96 | 44.1 | | |

2.3 General Behavior of an Aggregate Pier in Clayey Soil

Aggregate piers mainly derive their strength from the strength and stiffness of the surrounding soil that provides a confining pressure, due to the cohesionless nature of the aggregate of which they are comprised (Stuedlein). For such materials the value of c in Equation 2.1 is equal to zero. The confining pressures vary depending on the strength of the native soil and the presence of other aggregate piers or deep foundations. The

confining pressure increases in magnitude along the depth of the column due to the weight of the soil.

An aggregate pier is often built to support a spread footing carrying a structural load on inadequately strong native soil. Due to the greater stiffness of the aggregate pier the vertical stresses transferred from the footing will be concentrated into the aggregate pier and the vertical stresses of the native soil will decrease. As these stresses are transferred, the soil and pier will deform until the stresses reach equilibrium. Figure 2.6 illustrates the stresses on an aggregate pier. When the soil is normally consolidated, the foundation tends to increase in strength as excess pore water pressures are relieved by the drainage of water into the void spaces in the aggregate pier.

Stuedlein (2008) explains that an individual pier generally fails in one of two ways. The first occurs when the confining pressure is insufficient to resist the lateral loads from the pier. This results in the pier pushing out into the surrounding soil in the weakest areas and is called bulging because of the way in which the otherwise columnar pier develops a bulge. The second failure mode happens when the deeper layer upon which the pier is situated is not strong enough to withstand the vertical load transferred through the pier. This results in what is called basal punching as the pier punches through the underlying soil.

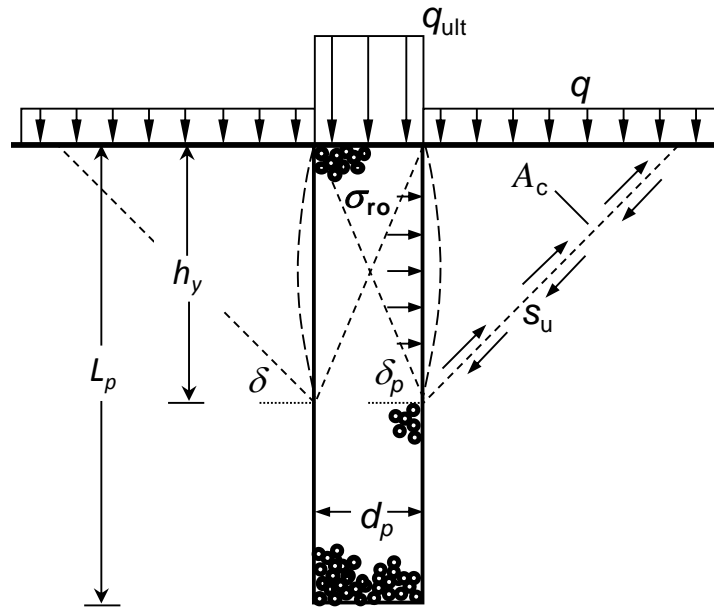


Figure 2.6 Stresses on a single, isolated aggregate pier (after Stuedlein and Holtz 2013)

2.4 Factors Affecting Bearing Capacity

The bearing capacity of an aggregate pier is affected by factors that arise from the material with which it is constructed, the material surrounding the pier, geometrical considerations, and loading boundary conditions. The material it is constructed with can vary in density, angularity, gradation, roughness, and mineral composition, and these factors can influence the ability of the pier to resist the axial loading. A denser pier is stronger than a looser pier, which is one reason why vibro-compaction is used often rather than other methods providing less densification. Higher angularities can lead to a stronger pier when the aggregate interlocks. However, if the aggregate breaks this can lead to a higher deflection. Roughness gives the aggregate more friction within the pier and with the surrounding soil, this allows the system to bear a greater load. Mineral composition is also important due to the different strength characteristics of the minerals

themselves. Some minerals also have the potential to dissolve in water, which makes them much less desirable as a building material. Much less is known about how the gradation of the aggregate affects the bearing capacity of a pier.

The surrounding soils are also a great contributor to the ability of the pier to bear the load. The confining pressure, water content, and the bearing capacity of the native soils impact the bearing capacity of the pier-soil system. At higher confining pressures the piers are able to bear larger loadings without failure. Similarly, the stronger the native soils, the greater the strength of the aggregate pier. A deeper footing embedment also leads to a stronger system. Water content mostly impacts the bearing capacity of the native soil, rather than directly affecting the pier itself. Inherent spatial variability of the strength and stiffness, which can depend on the water content in plastic fine-grained soils, can pose significant difficulty in the prediction of capacity. As such, the research on the factors affecting the bearing capacity of aggregate piers is ongoing as will be described herein.

2.5 Summary

Aggregate piers are an economically viable means of ground improvement for areas where the native soils are inadequate to support the load of new infrastructure. The most common methods of construction and failure of aggregate piers were described. Since crushed aggregate is typically used in the construction of aggregate piers the test results on the strength behavior of crushed aggregate from Duncan et al. (2007) were summarized. The bearing capacity of an aggregate pier is impacted by many factors and the prediction methods for calculating the bearing capacity are still often unreliable.

Thus, there is a need for additional research into how factors such as confining pressure affect the strength characteristics of an aggregate.

3.0 Research Objectives and Program

3.1 Research Objectives

The research objective was to determine the index and strength parameters for the limestone aggregate for use as a baseline in a study on the effect of cementation of the aggregate on the increase in the bearing capacity of aggregate piers. The specific objectives of this study include

1. Determination of a material gradation to be used for testing based on a particle size distribution of the aggregate as used in a previous study on aggregate piers;
2. Characterization of the index properties of the limestone aggregate; and,
3. Determination of the strength and stiffness of the limestone aggregate.

3.2 Research Program

The research program used to accomplish these objectives was as follows:

1. Mechanical sieving of the raw aggregate and batching into samples meeting the target gradation;
2. Determination of the minimum and maximum void ratios of the aggregate;
3. Development of specific compaction protocols for coarse-grained triaxial test specimen preparation based on a protocol from previous study using finer grained material;
4. Preparation of triaxial test specimens and loading specimens to failure under a variety of confining pressures; and,

5. Calculation of the strength and stiffness parameters for the limestone aggregate.

4.0 Triaxial Test Program

Triaxial testing is used to measure the strength of a material by simulating the stresses that it would be subjected to in-situ. The specimen is carefully loaded into a cylindrical chamber and a confining pressure applied, mimicking the pressures from surrounding soils at pre-determined depths. An axial displacement is slowly applied while the resulting axial load and volume change response of the specimen is measured. Each of the tests for this study was performed using a different magnitude confining pressure to analyze the elemental strength of an aggregate pier at a different depth along its length. This chapter describes the equipment used for the triaxial tests and the test methodology including sieving specimen preparation and mounting, consolidation, and axial loading.

4.1 Equipment

The equipment used for this study included a set of sieves and mechanical shakers; containers with volume equal to 5 gallons for aggregate particles corresponding to each sieve size, a Modified Proctor hammer, a 6-in diameter split mold, a custom aluminum compaction/mounting base, a membrane applicator; membranes, and a triaxial cell and experimental station designed for large specimens.

The triaxial station is shown in Figure 4.1 and consisted of a base platen, a top platen, a triaxial chamber, a linear variable displacement transducer, a pressure regulating system, a de-aired water system, a drainage system, a volume change device, a load cell and loading piston, a control panel, and a data acquisition computer.



Figure 4.1 Triaxial station

4.2 Test Methodology

4.2.1 Sieving Aggregates for Specimen Preparation

Aggregate was obtained from the Beckman Quarry of Martin Marietta Materials SW in Humble, Texas for this experimental study. This material was used to construct aggregate piers supporting 17 full-scale structural foundations for research investigations as reported by Stuedlein and Holtz (2012). Material was sieved using a mechanical shaker and the following sieve openings: 1", $\frac{3}{4}$ ", $\frac{5}{8}$ ", $\frac{1}{2}$ ", $\frac{3}{8}$ ", #4, and #8; note that the number following the numeral sign indicates the number of openings per square inch. Figure 4.2 shows the aggregate used in this study. Each aggregate size was sorted into a separate container and specimens were mixed then mixed by weight to meet a specific

test gradation as seen in Table 4.1, below. The test gradation was selected to meet the gradation used in the work by Stuedlein and Holtz (2012).



Figure 4.2 Aggregate used in this study

Table 4.1 Test gradation

| Sieve Size | Percent Passing (%) | Mass per specimen (kg) |
|-------------------|--------------------------------|-----------------------------------|
| 1" | 100.0 | 0.004 |
| 3/4" | 82.0 | 0.716 |
| 5/8" | 66.0 | 0.640 |
| 1/2" | 42.5 | 0.940 |
| 3/8" | 20.0 | 0.900 |
| #4 | 5.0 | 0.600 |
| #8 | 0.0 | 0.200 |

4.2.2 Specimen Preparation

Batches of aggregate were mixed to meet the target gradation. Water was added to the batched aggregate to meet the optimum water content of 6.4% determined in the compaction testing described in Section 5.2. The batch was mixed thoroughly by hand in a flat metal pan and continued throughout the compaction process in between successive lifts.

A sacrificial membrane was applied to the inside of the split mold to hold the shape of a specimen following removal of the mold and to separate the specimen from the pressurizing fluid. The large void spaces within the large, angular aggregate resulting from the uniform gradation meant that the specimens were unstable after compaction. The use of additional membranes and a special compaction base were necessary to mount the specimen into the triaxial apparatus with minimal disturbance of the material. The split mold was mounted onto the custom made compaction base and then the aggregate was added in lifts of 25 to 50 mm and compacted with a Modified Proctor hammer. It was determined that 11 lifts were generally necessary to fill the mold and generate a specimen. The specimen consolidated to 21 kPa effective confining pressure was compacted in only 10 lifts because the final lift would be too close to the rim of the mold for appropriate compaction. The compaction pattern used followed the procedures from ASTM D 1557-12 (ASTM 2012) for a 6-in proctor mold. Figure 4.3 shows the compacted specimen.



Figure 4.3 Compacted specimen on custom compaction base

4.2.3 Mounting the Specimen

The triaxial testing base was prepared by plugging the cell drainage holes to prevent material from becoming trapped in them. A porous stone which had been boiled for 10 minutes was placed on top of the base platen followed by a piece of pre-soaked filter paper. The compaction base was then placed such that the open curve of the compaction base lined up with the triaxial base. Three people were required to slide the specimen and split mold onto the triaxial base. Two people held the separate bases together firmly while the third carefully slid the mold along the compaction base and onto the triaxial base taking care to avoid sliding the filter paper off the stone or tearing it. Figure 4.4 shows this step.



Figure 4.4 Transfer of specimen from compaction base to triaxial base

Once the specimen was fully on the triaxial base, the compaction base was removed. Then as one person held the membrane down to the triaxial base, a second person carefully removed the split mold. The third person reached through the membrane applicator to hold the top of the compaction membrane and then lowered the applicator over the specimen as the split mold was removed. Once the membrane applicator was in place, the third person pushed the membranes onto the specimen using pressurized air. Additional membranes were used at higher confining pressures to prevent membrane puncture; three membranes were used for stresses above 101 kPa and four membranes for stresses above 257 kPa.

After the membrane was applied to the specimen, a second piece of pre-soaked filter paper was placed on top of the specimen followed by a porous stone and the loading platen. The platen was then leveled on the specimen to prevent the development of loading eccentricities and ensure uniform transmission of axial stress. The membrane was

then taken off the applicator and secured to the platens with rubber O-rings. Drainage lines were attached to the top and bottom platens creating a specimen drainage system. A 10 kPa vacuum was applied until air bubbles ceased to be released. The diameter and height of the specimen was measured along three locations to enable computation of the specimen volume. Thereafter, the drainage valves were closed to maintain the 10 kPa vacuum on the specimen and the vacuum system disconnected. The cell and platens were cleaned to remove debris, the plugs were removed, and the system checked for leakage and membrane puncture. Figure 4.5 shows the specimen with the top platen and drainage lines attached and vacuum applied.



Figure 4.5 Specimen with top platen, drainage lines and under vacuum

The triaxial chamber was carefully installed and the top piston inserted and threaded into the top platen and locked in place. Once secure, the triaxial chamber was filled with de-aired water so as to allow the application of cell pressure. Then, the drainage valves were opened and the vacuum on the specimen was released. Gaseous

carbon dioxide (CO₂) was pumped through the specimen from the base of the triaxial chamber to displace air that might exist in the void spaces. Thereafter, de-aired water pumped into the specimen from the base to saturate the specimen. Figure 4.6 shows the specimen as the CO₂ was being flushed through it.

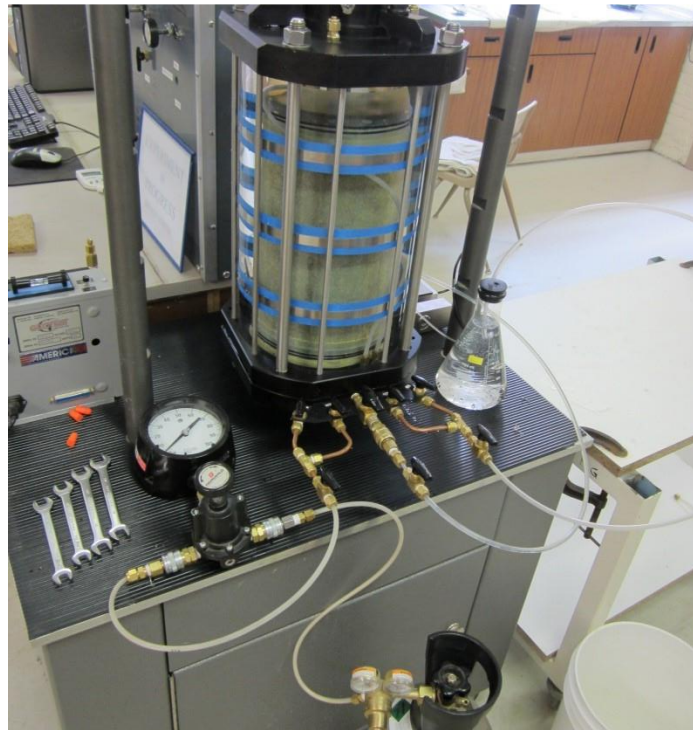


Figure 4.6 Specimen during CO₂ flush (from Walters)

4.2.4 Specimen Shearing Procedures

In order for the measurement of the volume change of the specimen to be accurate the specimen must be fully saturated. The volume change is measured by the water, which responds in a relatively incompressible manner for the pressures investigated, that drained out of the specimen during shearing. The presence of air in the specimen would indicate that the specimen exhibits less volume change and stiffness than in actuality.

Thus, before the specimen was subjected to consolidation and shearing, saturation tests were performed to ascertain the saturation of the specimen.

The B-value is the ratio of the change in pore water pressure to the change in confining stress applied to a specimen with drainage valves closed (i.e., undrained loading). For a fully-saturated soft clay, the B-value is 1, more stiff materials such as the limestone aggregate used in this study are fully-saturated at a value slightly less than 1 owing to the significantly greater soil-skeleton stiffness. For this study, a value above 0.93 was considered acceptable based on Holtz et al. (2011). If the value was too low, the back pressure was increased slightly and then the B-value calculated again.

Once an acceptable value was reached the specimen was consolidated at the appropriate confining pressure and allowed to reach equilibrium. Specimens were loaded at a rate of approximately 0.25% axial strain per minute and the displacement, axial load and volume change were recorded. After failure, specimens were unloaded and the sample was oven-dried and weighed to determine the actual initial void ratio.

5.0 Results

This chapter describes the grain size distribution, the minimum and maximum void ratios, and the compaction characteristics of the aggregate evaluated in this study. The constitutive properties of the aggregate are reported, including the principal stress difference-axial strain and volumetric strain-axial strain relationships, along with a discussion of the stiffness of the aggregate. Hyperbolic model parameters as outlined in Duncan et al. (1980) are calculated and stress-strain curves fit to the model. The peak and residual friction angles are reported for each test. A comparison to the results of the Duncan et al. (2007) aggregate testing is included in Section 5.4 to compare the results and confirm their validity.

5.1 Grain Size Distribution

The aggregate received from the quarry had particle sizes ranging from less than 7.5 μm to 22.4 mm. The analysis of the grain size distribution found that the coefficient of uniformity, C_u , was 2.31 and the coefficient of curvature, C_c , was 1.09. According to ASTM D 2487-11 (ASTM 2011) aggregates with these parameters are classified as a poorly-graded gravel (GP). Figure 5.1 shows the grain size distribution. The specific gravity, G_s , was calculated to be 2.701.

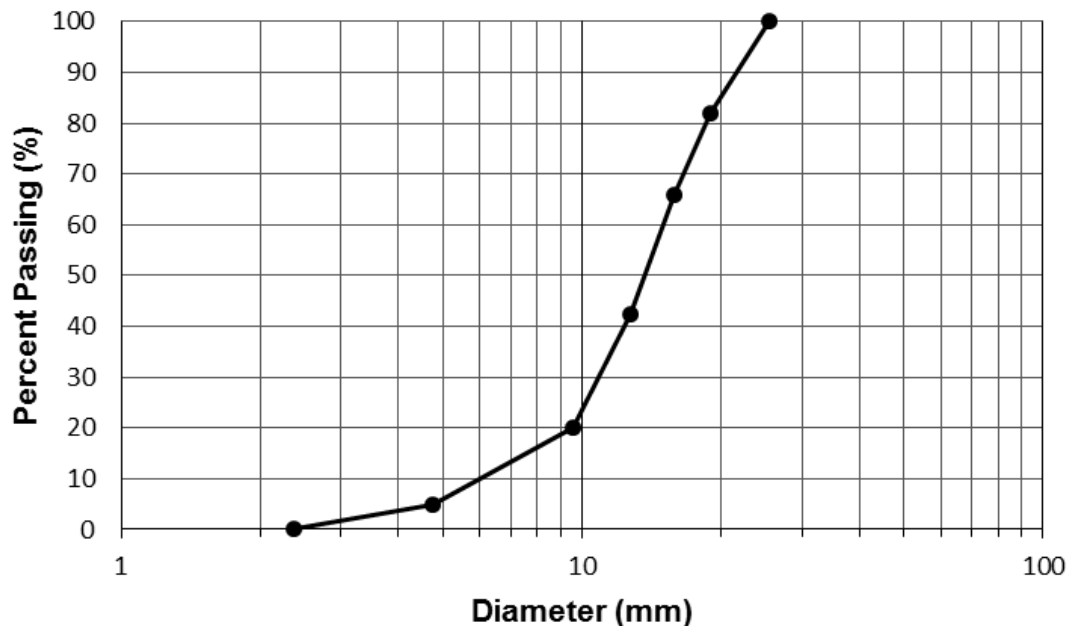


Figure 5.1 Grain Size Distribution

5.2 Minimum and Maximum Void Ratio and Compaction Characteristics

The minimum and maximum void ratios correspond with the theoretical minimum and maximum densities that a specimen with a specific gradation of particles can have. A void ratio is defined as the ratio of the volume of the void space, which is typically filled with air and/or water, and the volume of the solid particles in a given specimen. When a specimen is compacted to the minimum void ratio, then no further increases in density are possible; on the other hand, when a specimen exists at the maximum void ratio, it is in the loosest possible state possible. The maximum void ratio was determined by loosely dumping aggregate into a 6 in Proctor mold and then measuring the mass following the ASTM D 4254-00 (Reapproved 2006; ASTM 2006b) procedure. This was repeated ten times, and once it was concluded that the results were representative of the true value, the average was taken as the representative maximum void ratio. The maximum void ratio,

e_{max} , was determined equal to 1.01 with a standard deviation of 0.021. The results of the individual trials are presented in Table 5.1.

Table 5.1 Maximum Void Ratio Trials

| Trial | Mass (kg) | e_{max} |
|--------------------|-----------|-----------|
| 1 | 2.905 | 0.99 |
| 2 | 2.834 | 1.04 |
| 3 | 2.856 | 1.02 |
| 4 | 2.878 | 1.01 |
| 5 | 2.859 | 1.02 |
| 6 | 2.880 | 1.00 |
| 7 | 2.855 | 1.02 |
| 8 | 2.843 | 1.03 |
| 9 | 2.935 | 0.97 |
| 10 | 2.882 | 1.00 |
| Average | 2.873 | 1.01 |
| Standard Deviation | | 0.021 |

The ASTM D 5453-00 (Reapproved 2006; ASTM2006a) standard is also used to determine the minimum void ratio, but is only appropriate for smaller sized, less angular aggregate. This method involves placing the aggregate within a mold, adding a pre-defined surcharge to the top of the specimen, and placing the assembly on a vibrating table for a period of 8 minutes at 60 Hz or 12 minutes at 50 Hz. Due to the angularity of the aggregate and its ability to interlock with other particles, vibration was deemed unsuitable for this material. Hand construction of a compact specimen was tried, but was also determined to be insufficient. Instead, the minimum void ratio, e_{min} , was back calculated from the determination of the maximum dry unit weight and the specific gravity of the aggregate.

The relationship between the dry unit weight and water content for this aggregate was determined using the Modified Proctor Test Method C from ASTM D 1557-12

(ASTM 2102). The relationship is shown in Figure 5.2. Method A requires that less than 25 percent by mass be retained on the #4 (4.75 mm) sieve, and Method B requires that less than 25 percent by mass be retained on the 0.375 in (9.53 mm) sieve. The aggregate for this study exceeded both of these requirements. Method C was used because it fit the particle size and mold requirements for the test. Method C excludes particles greater than 0.75 in (19 mm), but an oversize correction factor can be applied to the results.

Figure 5.2 presents the compaction curve generated for this aggregate; based on the data, a maximum dry unit weight of 18.4 kN/m^3 and an optimum water content of approximately 6.4 percent were determined for these aggregates. After the oversize correction factor from ASTM D 4718-87 (Reapproved 2007; ASTM 2007), the dry unit weight was 19.5 kN/m^3 . The minimum void ratio was back calculated using the uncorrected value of 18.4 kN/m^3 and the specific gravity of 2.701, and was determined to be 0.44. For clean sands, Youd (1973) states that the specific particle size is not a significant factor in void ratios. Variables such as the gradation, particle shape, and range in size are considered to contribute most to the possible ranges in void ratio. The minimum and maximum void ratios of a variety poorly-graded sands determined by Youd (1973) ranged from 0.271 to 0.803 and 0.491 to 1.42, respectively. Both the minimum and maximum void ratios determined in this study fall within the ranges found by Youd (1973).

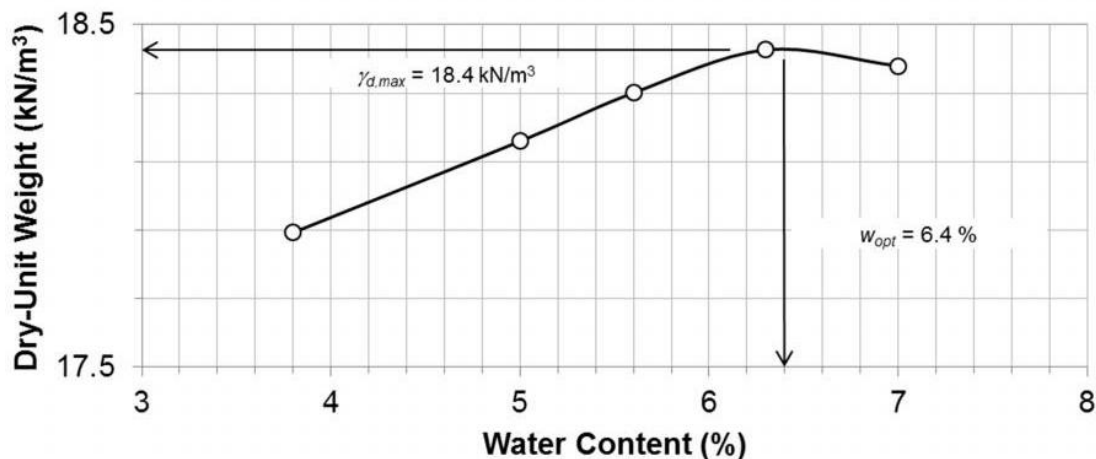


Figure 5.2 Modified Proctor compaction curve (from Newton 2014)

5.3 Constitutive Properties of the Aggregate

Five consolidated-drained triaxial tests were performed on limestone aggregate with a range of confining pressures. For this study, failure is defined by the peak principal stress difference, q_f , which is the maximum difference between σ'_1 and σ'_3 and the maximum principal stress ratio, which is the maximum ratio of σ'_1 and σ'_3 . As such, failure is defined in terms analogous to bearing failure, rather than displacement.

The effective confining stresses for the five tests were targeted to 20 kPa, 50 kPa, 100 kPa, 250 kPa, and 375 kPa. These effective confining stresses were chosen as representative of the confining stresses that might be experienced by an aggregate pier under service and failure conditions in the field. The tests model the elemental behavior of a singly-loaded aggregate pier resting on a firm bearing layer. The failure mode for such an aggregate pier is termed “bulging”, similar to the mode of failure for the aggregate in the triaxial test. Table 5.2 shows the actual effective confining stresses of the five tests and the pre- and post-consolidation relative densities, D_r . The relative densities

were calculated using the void ratios determined for pre- and post-consolidation. The void ratios were determined using the volume calculated before consolidation and the change in volume determined by the water displaced during the test and the mass of the solids. As indicated in Table 5.2, the pre-consolidation relative densities fell within a range of 64 to 77 percent, and are described as “dense” using accepted soil mechanics terminology. After the specimen was sheared the sample was oven dried and the sample weighed to determine the mass of the solids. The target post-consolidation relative densities were between 65 and 85 percent, which represents the lower bound of the typical magnitude of compaction in a full size aggregate pier. Duncan, et al. (2007) reported that the relative density of the #57 aggregate between 67 and 95 percent had little impact on the strength of the material owing to the more significant effect of particle angularity on strength for this uniformly-graded material. As shown in Table 5.2, the target post-consolidation relative densities were achieved.

Table 5.2 Effective Confining Stress and Pre and Post Consolidation Relative Density

| Effective confining Pressure, σ'_3 (kPa) | Pre- consolidation void ratio, e | Pre- consolidation relative density, D_r (%) | Post- consolidation void ratio, e | Post- consolidation relative density, D_r (%) |
|---|--|--|---|---|
| 21 | 0.644 | 63.8 | 0.631 | 66.0 |
| 48 | 0.638 | 64.9 | 0.606 | 70.5 |
| 101 | 0.616 | 68.7 | 0.584 | 74.3 |
| 257 | 0.594 | 72.6 | 0.589 | 73.4 |
| 375 | 0.571 | 76.6 | 0.515 | 86.4 |

5.3.1 Experimental Stress-Strain Response

The relationship between the effective principal stress difference and axial strain for each triaxial is shown in Figure 5.3. Each test exhibited moderate strain-softening behavior. Strain-softening means that upon reaching a maximum or peak principal stress difference (indicating failure), the stress difference gradually decreases with increases in the axial strain. The curves do not demonstrate a distinctive peak effective stress difference, and the decrease in stresses is gradual. The steepness of the stress-strain curves is an indication of its stiffness of the material; a steeper curve indicates a stiffer material. As shown below, the material demonstrated a higher stiffness at higher effective confining pressures. Additionally, the principal stress difference at failure occurred at higher corresponding axial strains for higher confining pressures, indicating that specimens with a higher confining pressure were able to sustain larger axial strains before reaching failure. Holtz et al. (2011) states that shear strength will increase with higher confining pressures. Lee (1965) performed a series of triaxial tests on poorly-graded Sacramento River sand at different confining pressures and determined that a higher confining pressure correlated with a larger principal stress difference at failure. Higher confining pressures correspond with higher relative densities and stronger particle interlock, which allows the material to demonstrate more stiffness and resistance to strain. The axial strain at failure ranged between 4.1 to 11.3 percent as seen in Figure 5.4. The individual tests results can be found in Appendix A. The Young's Modulus for each specimen was calculated and plotted in Figure 5.5. The values of the Young's Modulus ranged from 13 MPa to 94 MPa.

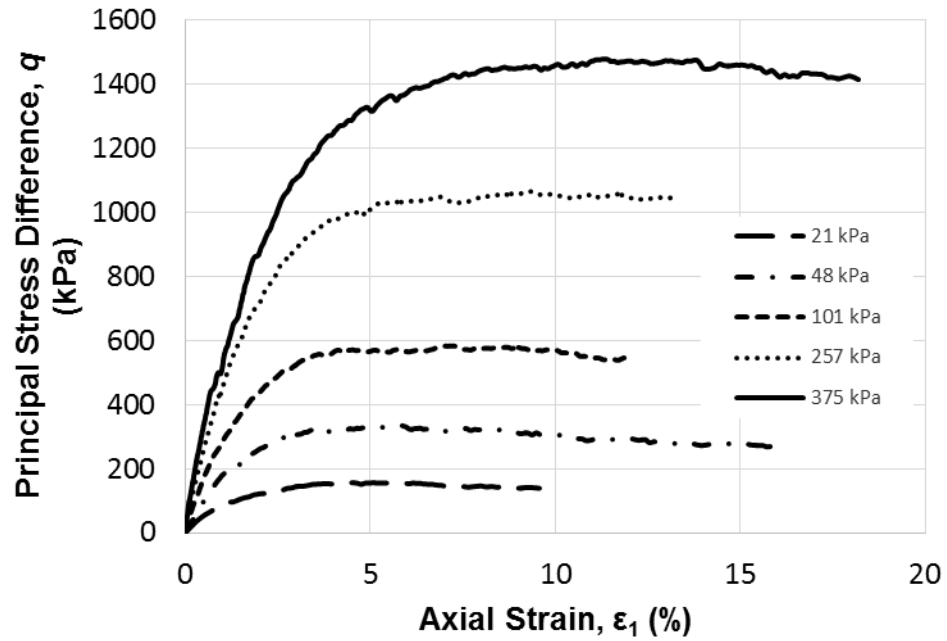


Figure 5.3 Principal stress difference, q , versus axial strain, ϵ_1

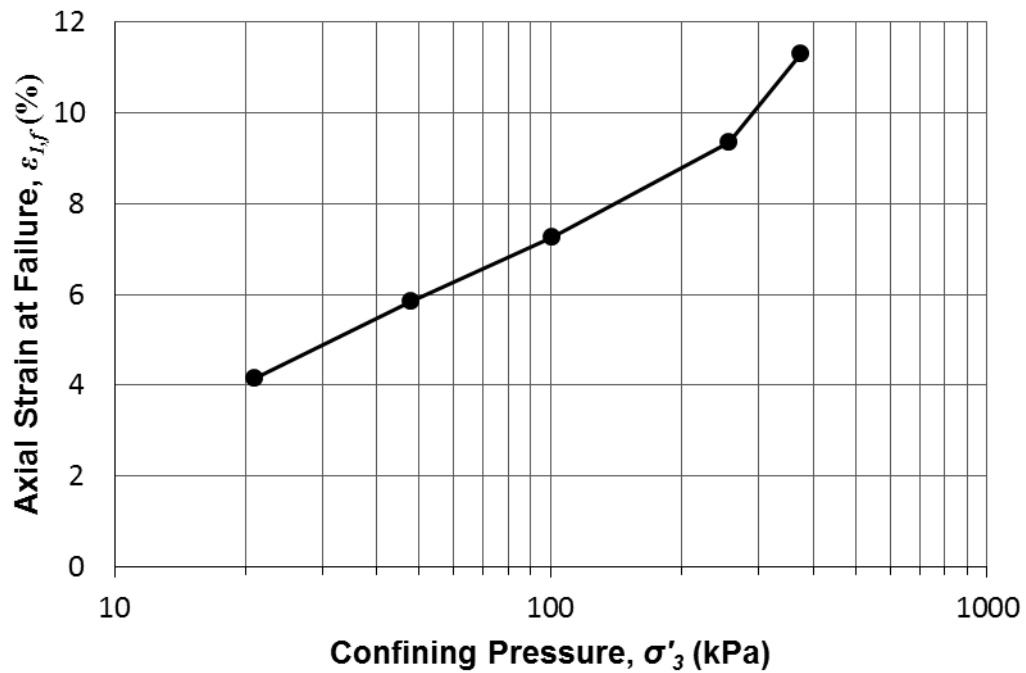


Figure 5.4 Axial Strain at failure vs Confining Pressure

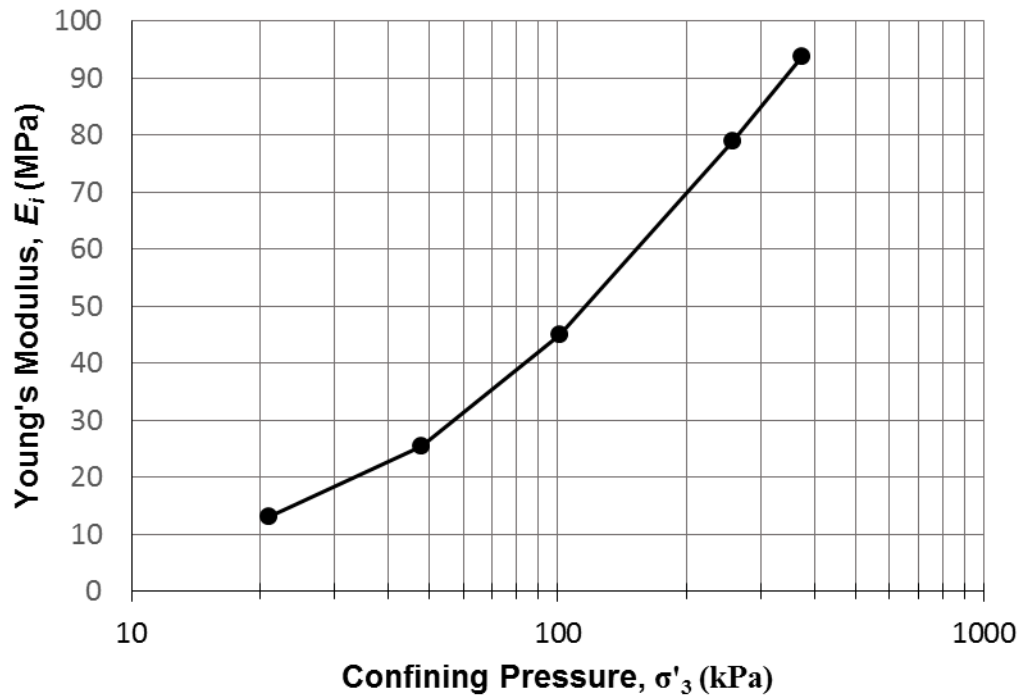


Figure 5.5 Young's Modulus vs Confining Pressure

5.3.2 Volumetric Strain- Axial Strain Response

During consolidated–drained triaxial tests, volume change of the specimen is allowed to occur and is measured to gauge the dilation response of the specimen. Tests performed by Duncan et al. (2007) showed that the limestone aggregate demonstrated a dilatant volume change response at lower confining pressures, while at high confining pressures the specimens did not exhibit dilation. Dilation is the movement of particles over one another during compression, which results in an expansion in volume. At higher confining pressures, the aggregate encounters difficulty overcoming the particle interlock, and this impedes particle movement and inhibits dilation. Figure 5.6 shows the family of volumetric strain-axial strain for the tests performed in this study. Four of the five tests exhibited dilatant behavior. A specimen under compression has an initial tendency to contract. However, when the particles begin to rub against one another and

encounter resistance to additional compression they will move up and over each other which causes the material to expand in volume under higher axial strains. Only the highest confining pressure, with an effective confining stress of 357 kPa, was high enough to prevent dilation. The specimen sheared at 357 kPa demonstrated continuous compression with no dilatant behavior.

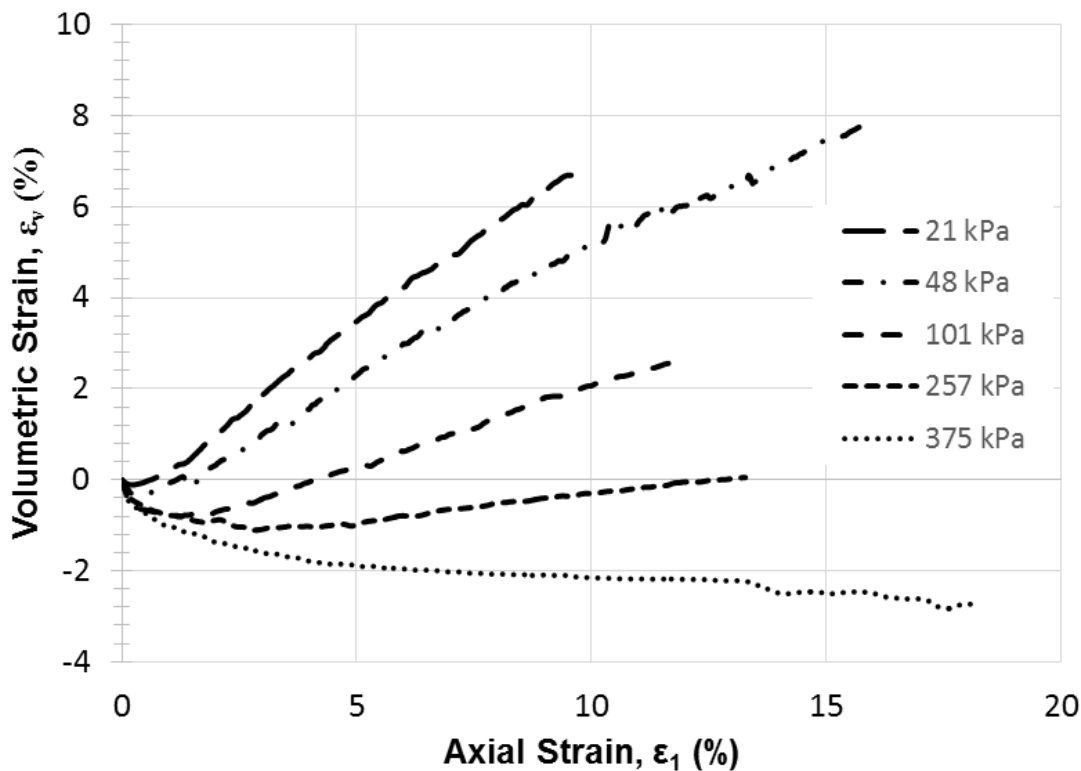


Figure 5.6 Volumetric Strain, ϵ_v , versus axial strain, ϵ_1

5.3.3 Hyperbolic Model Parameters from Duncan et al. (1980)

The methods from Duncan et al. (1980), based on Duncan and Chang (1970), were followed to fit the experimental stress-strain data from each test to a hyperbolic stress-strain model, termed the Duncan-Chang model. The Duncan-Chang model simulates the stress-strain behavior under static soil conditions. The hyperbolic parameters determined with this method are derived for fitting the laboratory data to a

hyperbolic curve and do not represent specific soil properties. However, according to Duncan et al. (1980), the parameters depend on the range of confining stress, soil density, water content and drainage conditions, and as such the test conditions should closely approximate the field conditions. Duncan et al. (1980) also specifies that the hyperbolic curves are appropriate for modeling up to the point of failure, but may not be accurate after the failure point depending on the severity of the changes in soil response as a result of failure. The hyperbolic relationships also do not account for volumetric changes due to dilation, and may exhibit limited accuracy for highly dilatant soils.

Duncan et al. (1980) suggests that the principal stress difference and axial strain at 70 and 95 percent of the principal stress difference at failure be used for fitting hyperbolic curves to the test data. These values are used in conjunction with the confining pressure to find the parameters for the hyperbolic curve. Equation 5.1 defines the hyperbolic stress difference in relation to axial strain:

$$(\sigma_1 - \sigma_3)_{hyp} = \frac{\varepsilon_1}{\frac{1}{E_i} + \frac{\varepsilon_1}{(\sigma_1 - \sigma_3)_{ult}}} \quad (5.1)$$

where $(\sigma_1 - \sigma_3)_{hyp}$ is the fitted hyperbolic stress difference, ε_1 is the axial strain, E_i is the initial tangent modulus, and $(\sigma_1 - \sigma_3)_{ult}$ is the asymptotic stress difference.

The asymptotic stress difference is found using Equation 5.2:

$$\frac{1}{(\sigma_1 - \sigma_3)_{ult}} = \frac{\frac{\varepsilon_{1,95\%}}{(\sigma_1 - \sigma_3)_{95\%}} - \frac{\varepsilon_{1,70\%}}{(\sigma_1 - \sigma_3)_{70\%}}}{\varepsilon_{1,95\%} - \varepsilon_{1,70\%}} \quad (5.2)$$

where $\varepsilon_{1,95\%}$ and $\varepsilon_{1,70\%}$ are the axial strains at 95 and 70 percent of the principal stress difference at failure, and $(\sigma_1 - \sigma_3)_{95\%}$ and $(\sigma_1 - \sigma_3)_{70\%}$ are 95 and 70 percent of the principal stress difference at failure.

The initial tangent modulus is found using Equation 5.3:

$$\frac{E_i}{P_a} = \frac{2.0}{\frac{\varepsilon_{1,70\%}}{(\sigma_1 - \sigma_3)_{70\%}} + \frac{\varepsilon_{1,95\%}}{(\sigma_1 - \sigma_3)_{95\%}} - \frac{1}{(\sigma_1 - \sigma_3)_{ult}} (\varepsilon_{1,70\%} + \varepsilon_{1,95\%})} \frac{1}{P_a} \quad (5.3)$$

where P_a is the atmospheric pressure. The table containing the values resulting from these equations can be found in Appendix B. Figures 5.7 through 5.11 plot the hyperbolic stress-strain curve with the actual stress-strain curve for each of the tests.

For the lower confining stresses, up to 101 kPa, the hyperbolic curve closely models the actual curve up to approximately 3.5 percent axial strain. For the specimen sheared at 257 kPa the hyperbolic curve was accurate up to approximately 6.0 percent axial strain, and for the specimen sheared at 375 kPa the hyperbolic curve demonstrated close agreement with the actual curve up to approximately 8.5 percent axial strain. Thus, the Duncan-Chang hyperbolic may be used to simulate stresses up to the strains where the fitted and observed stress-strain curves diverge.

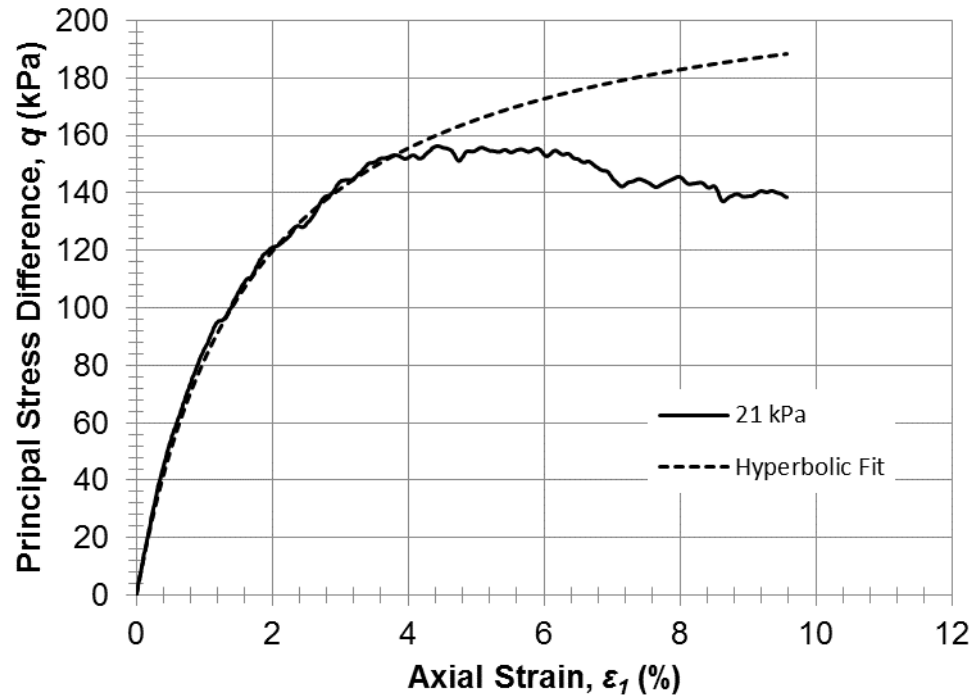


Figure 5.7 Hyperbolic stress-strain curve compared to actual stress-strain curve for 21 kPa confining stress

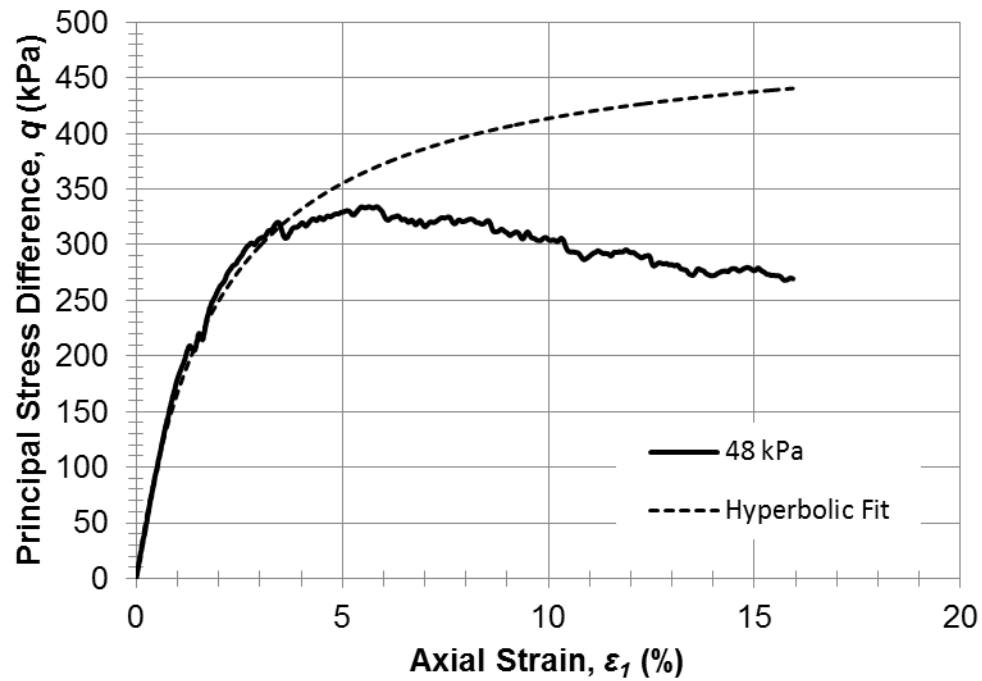


Figure 5.8 Hyperbolic stress-strain curve compared to actual stress-strain curve for 48 kPa confining stress

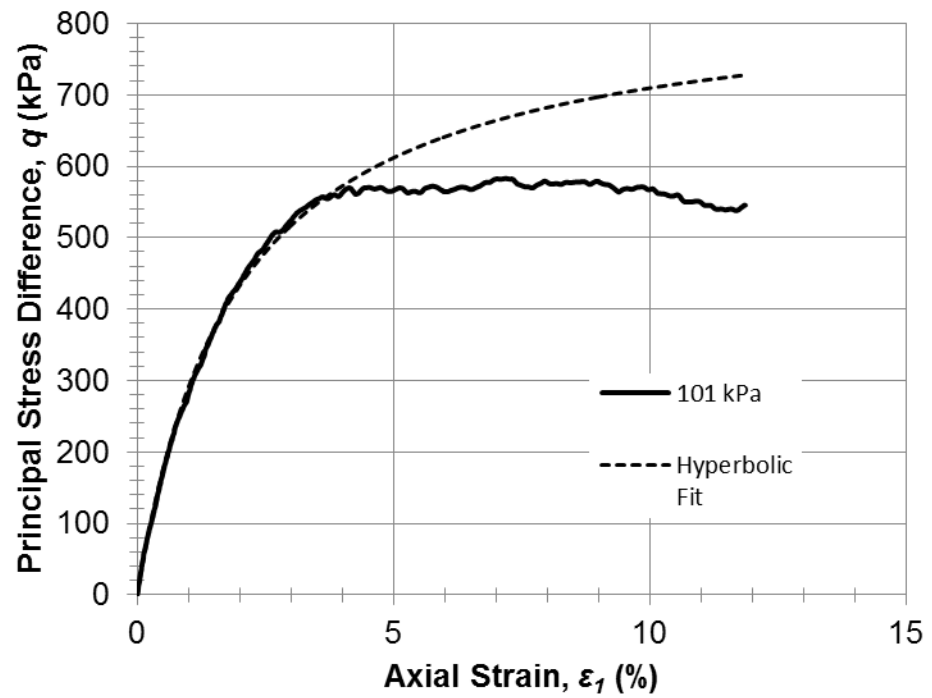


Figure 5.9 Hyperbolic stress-strain curve compared to actual stress-strain curve for 101 kPa confining stress

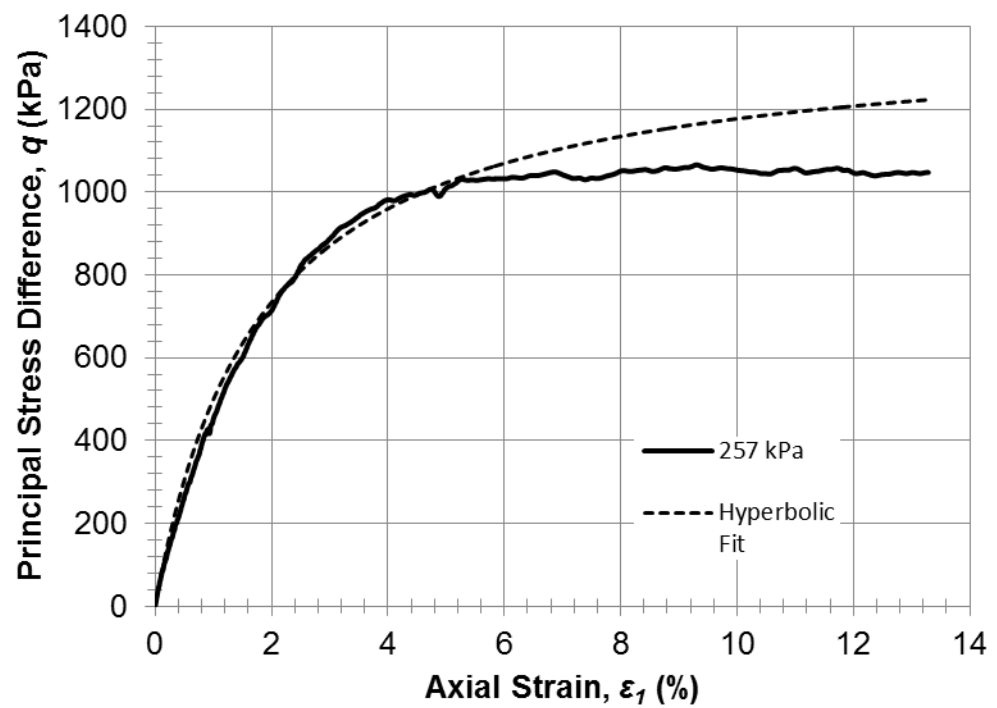


Figure 5.10 Hyperbolic stress-strain curve compared to actual stress-strain curve for 257 kPa confining stress

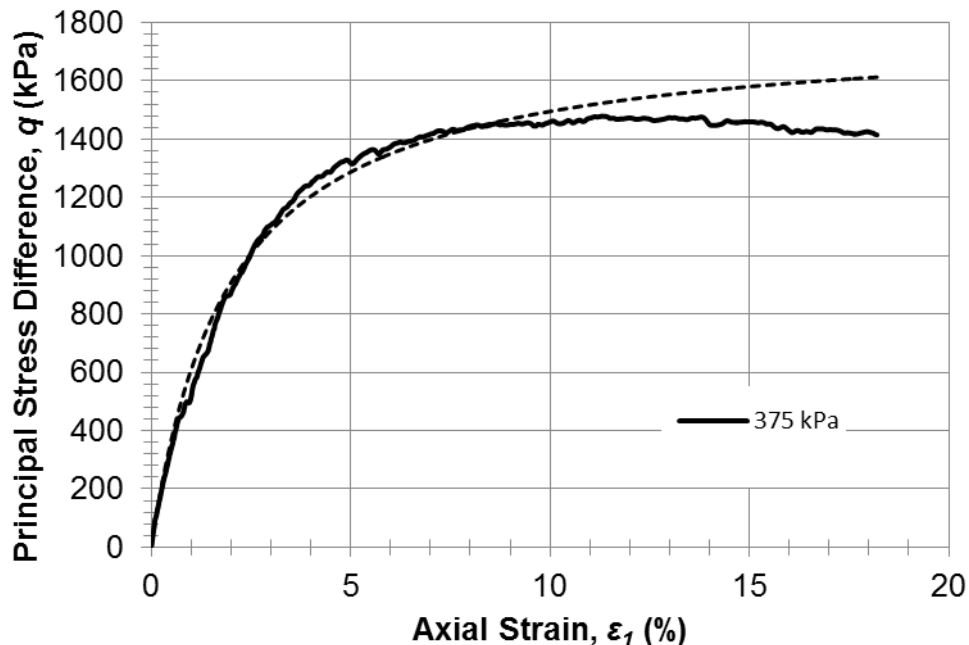


Figure 5.11 Hyperbolic stress-strain curve compared to actual stress-strain curve for 375 kPa confining stress

5.3.4 Peak and Residual Friction Angles

The friction angle, or angle of internal friction, is the slope of the Mohr-Coulomb failure envelope, and is one of the strength parameters for a material. Equation 5.4 details how the friction angle can be calculated using the principal stresses at failure:

$$\phi' = \arcsin\left(\frac{\sigma_{1f} - \sigma_{3f}}{\sigma_{1f} + \sigma_{3f}}\right) \quad (5.4)$$

The peak and residual friction angles for each of the tests were calculated. The peak friction angle is the angle of internal friction at failure and displays the materials greatest strength. The residual friction angle is indicative of the strength that remains after failure as defined in this study. The results, as shown in Figure 5.12, demonstrate a semi-logarithmic relationship between confining stress and friction angle. The peak friction angle ranged from 52.9 degrees for the lowest confining pressure to 41.6 degrees

for the highest confining pressure. The residual friction angle ranged from 49.1 to 40.8 degrees for the lowest and highest confining pressures, respectively. The minor difference in peak and residual friction angles is a result of the relatively small strain-softening response shown in Figure 5.3 in Section 5.3.1. The lower confining stresses demonstrate a slightly larger difference between the peak and residual friction angles due to the increased dilation response in lower confining pressures. The higher confining stresses demonstrated very little difference. This can likely be ascribed to the less dilative, or fully compressive, response of the material at higher confining pressures.

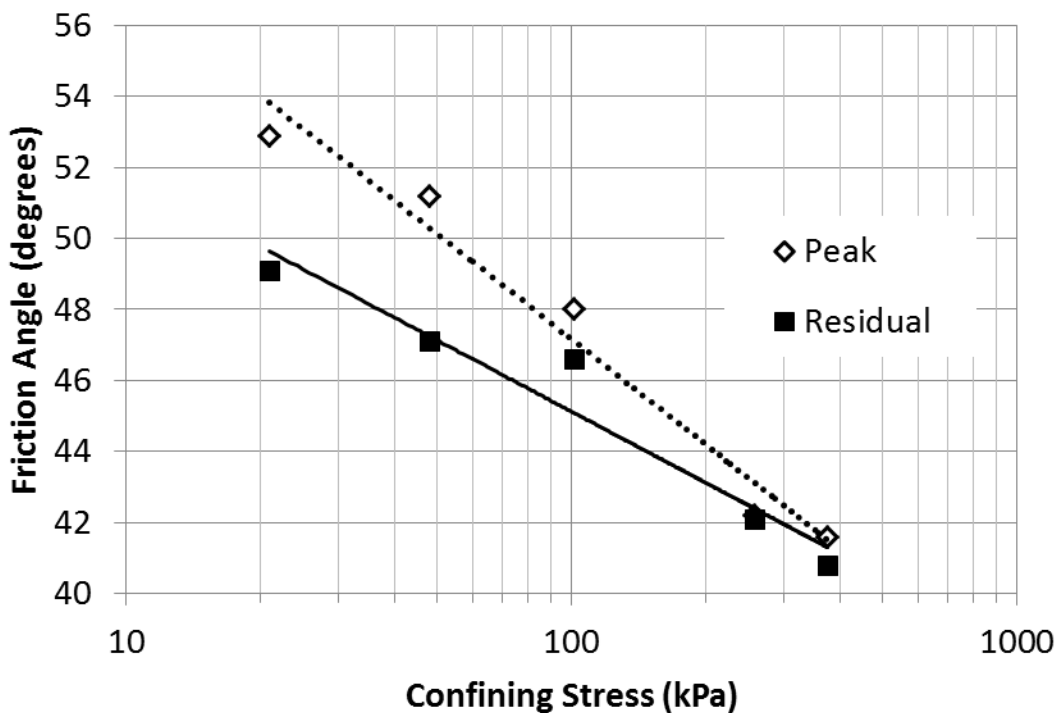


Figure 5.12 Peak and Residual Friction Angles versus Confining Stress

5.4 Stress-strain and Volumetric Strain Response of the Aggregate in Comparison to Duncan et al. (2007)

The stress-strain and volumetric strain response for the tests in this study were compared to the results of the tests on the #57 aggregate reported by Duncan et al. (2007) due to the similarities of the aggregates. The gradations of the two aggregates are compared below in Figure 5.13. The gradations are similar and suitable for use in strength comparisons; however, it is noted that the gradation used in this study is constituted with a greater amount of fine aggregates.

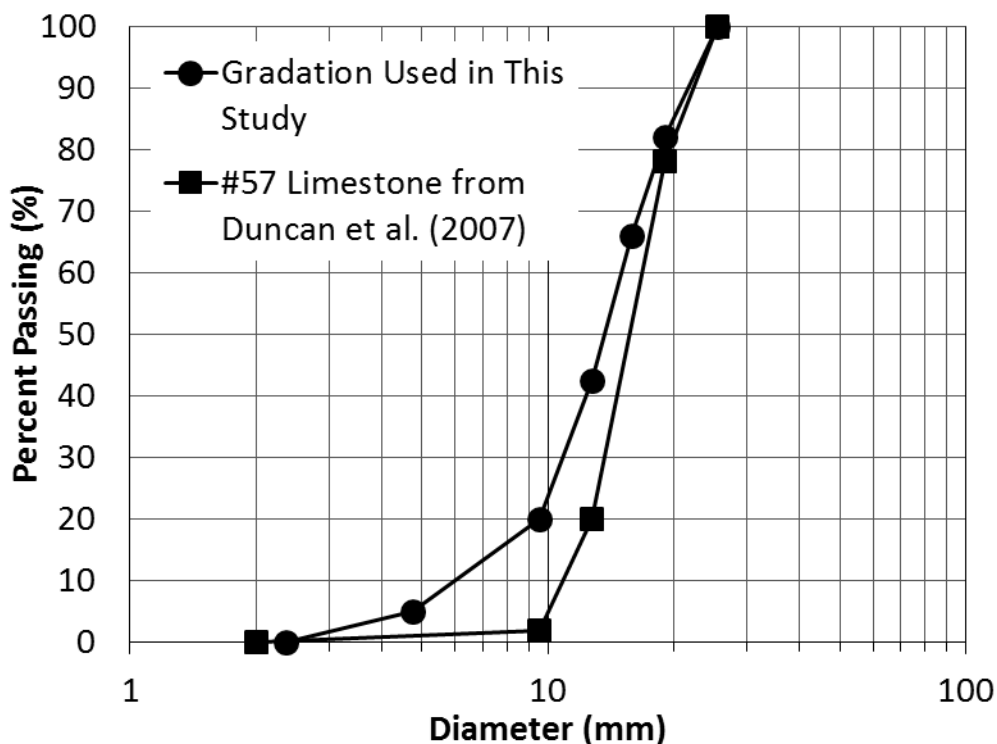


Figure 5.13 Aggregate gradation used in this study as compared to #57 limestone gradation from Duncan et al. (2007)

The stress-strain relationships of three tests from Duncan et al. (2007) are compared to tests with similar confining pressures from this study in Figures 5.14 to 5.16. These tests also display strain softening, although the tests were not continued as far past

the point of failure as the tests for this study. Similar to the results of this study, the specimens sheared at higher confining pressures demonstrated steeper curves and larger principal stress differences at failure. Volumetric strain-strain curves for these comparisons are shown in Figures 5.17 through 5.19. Each of the tests displayed dilatant behavior with initial compression followed by an expansion in volume with increasing axial strains. The highest confining pressure used by Duncan et al. (2007) on the #57 limestone was 208.7 kPa, which is compared to the test run at a confining pressure of 250 kPa in this study.

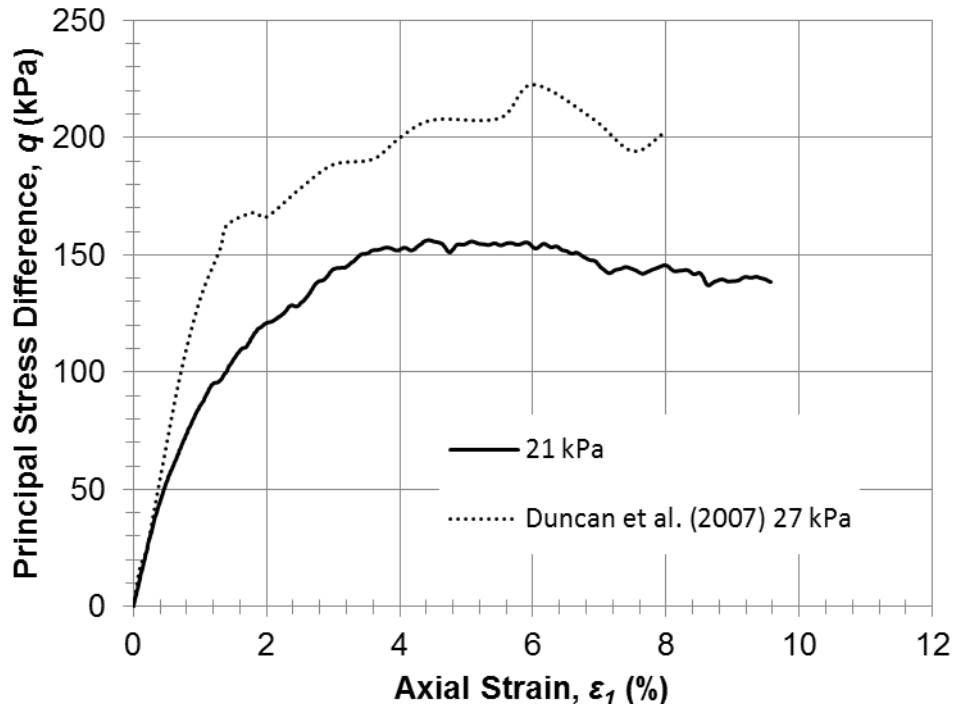


Figure 5.14 Principal stress difference versus axial strain for 21 kPa confining pressure from this study compared to 27 kPa confining pressure from Duncan et al. (2007)

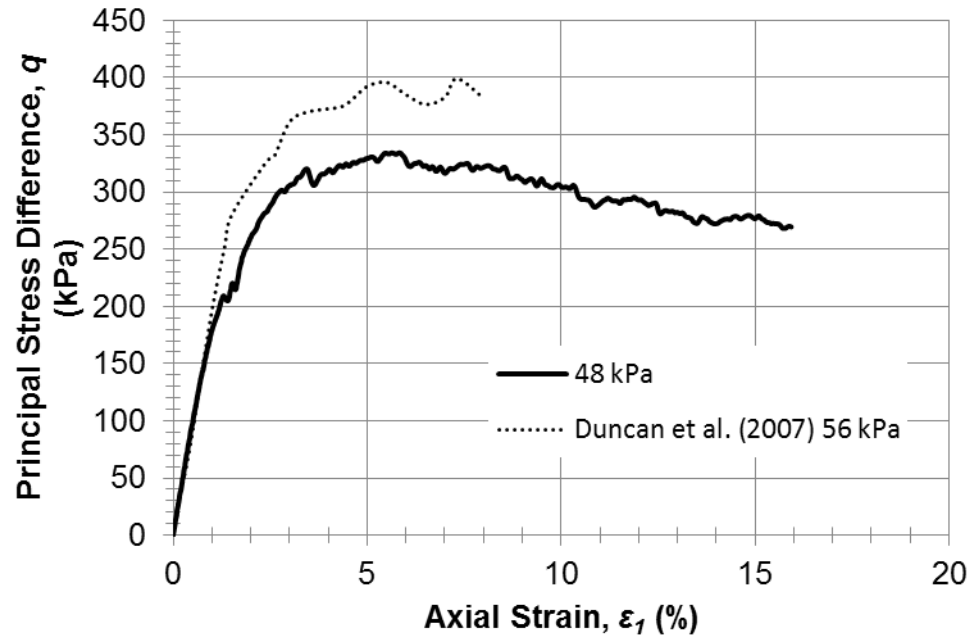


Figure 5.15 Principal stress difference versus axial strain for 48 kPa confining pressure from this study compared to 56 kPa confining pressure from Duncan et al. (2007)

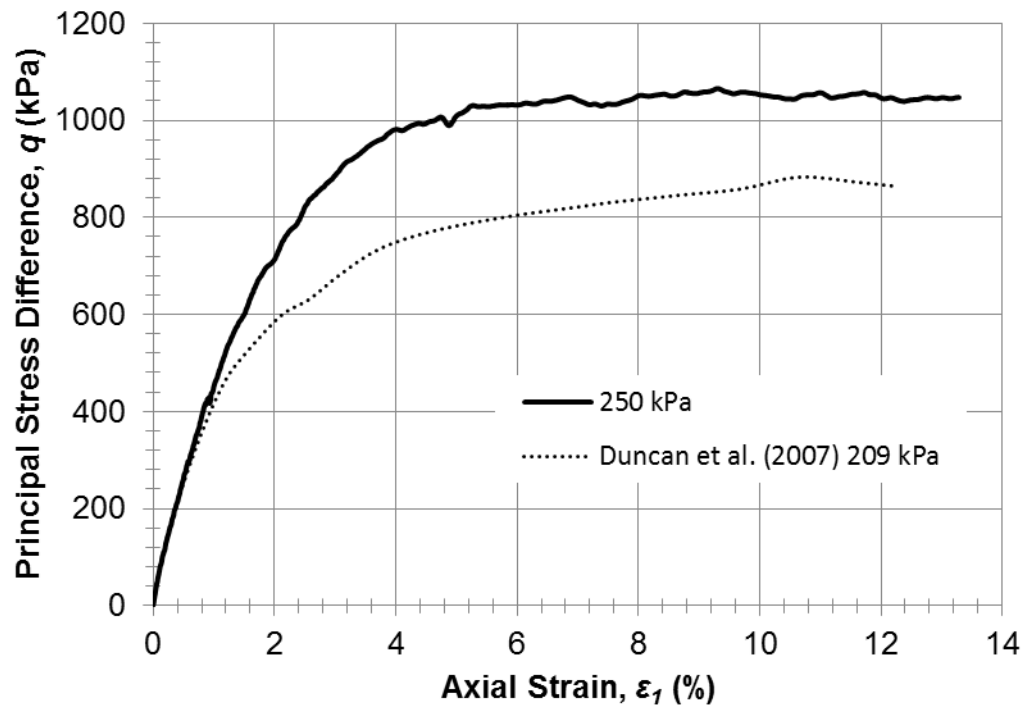


Figure 5.16 Principal stress difference versus axial strain for 250 kPa confining pressure from this study compared to 209 kPa confining pressure from Duncan et al. (2007)

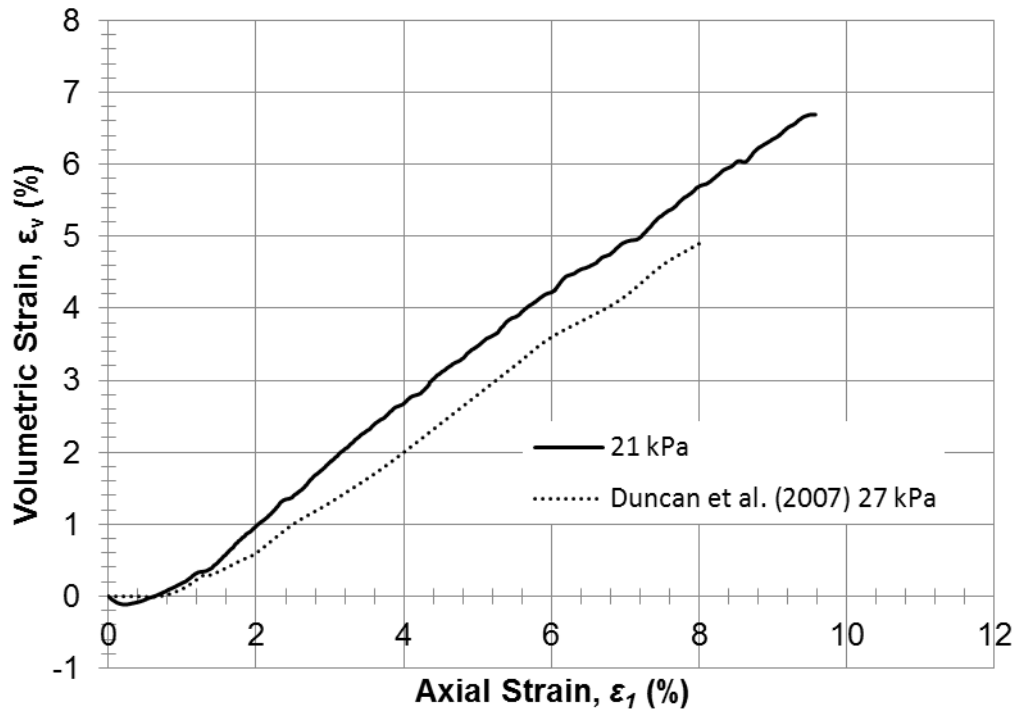


Figure 5.17 Volumetric strain versus axial strain for 21 kPa confining pressure from this study compared to 27 kPa confining pressure from Duncan et al. (2007)

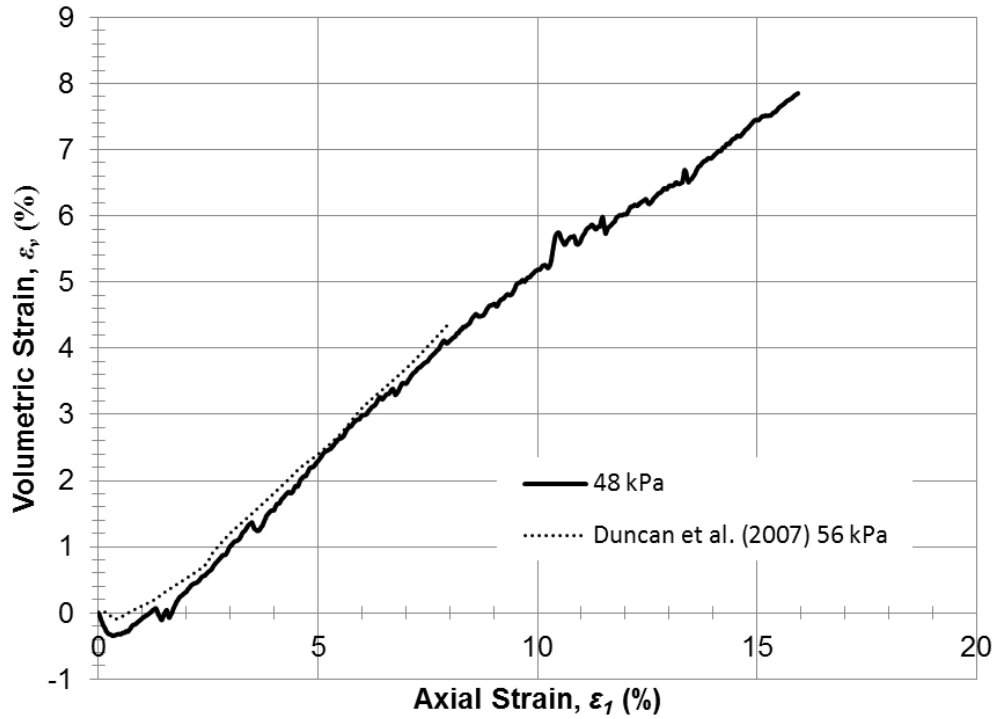


Figure 5.18 Volumetric strain versus axial strain for 48 kPa confining pressure from this study compared to 56 kPa confining pressure from Duncan et al. (2007)

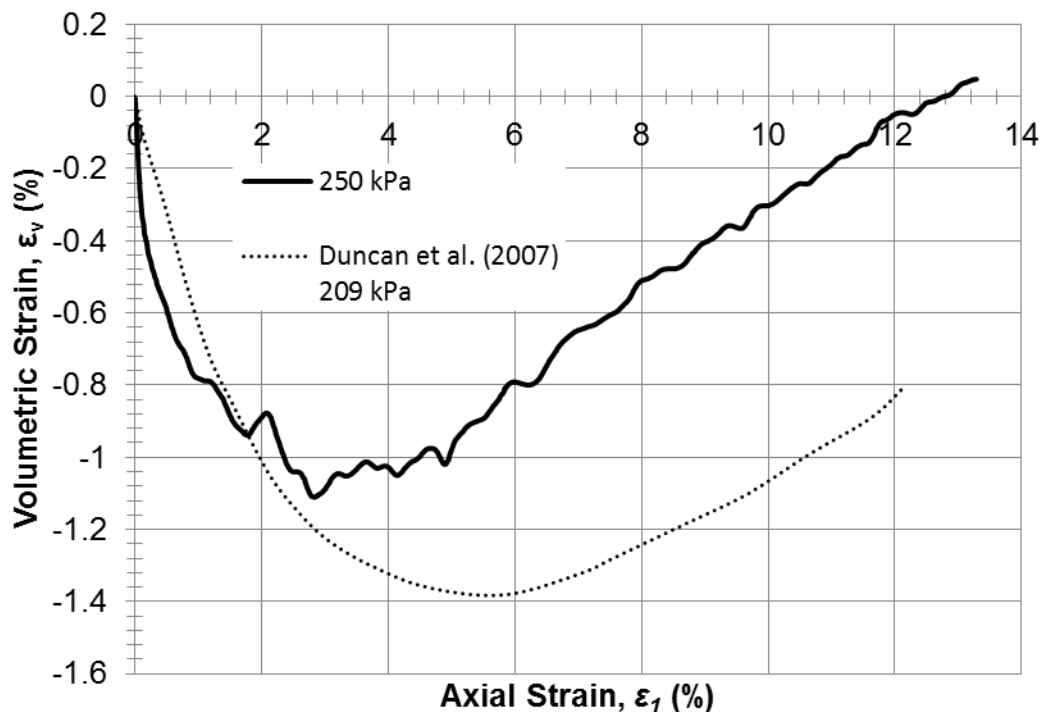


Figure 5.19 Volumetric strain versus axial strain for 250 kPa confining pressure from this study compared to 209 kPa confining pressure from Duncan et al. (2007)

Peak friction angles generated from this study are compared to the friction angles of the #57 limestone from Duncan et al. (2007). This comparison is shown in Figure 5.20. The variation in the friction angle with effective confining stress for the two gradations is similar. Duncan et al. (2007) concluded that the friction angle did not vary significantly within a large range of relative densities because other factors such as the angularity had a much greater impact than density. The test data developed in this study appears to confirm this finding.

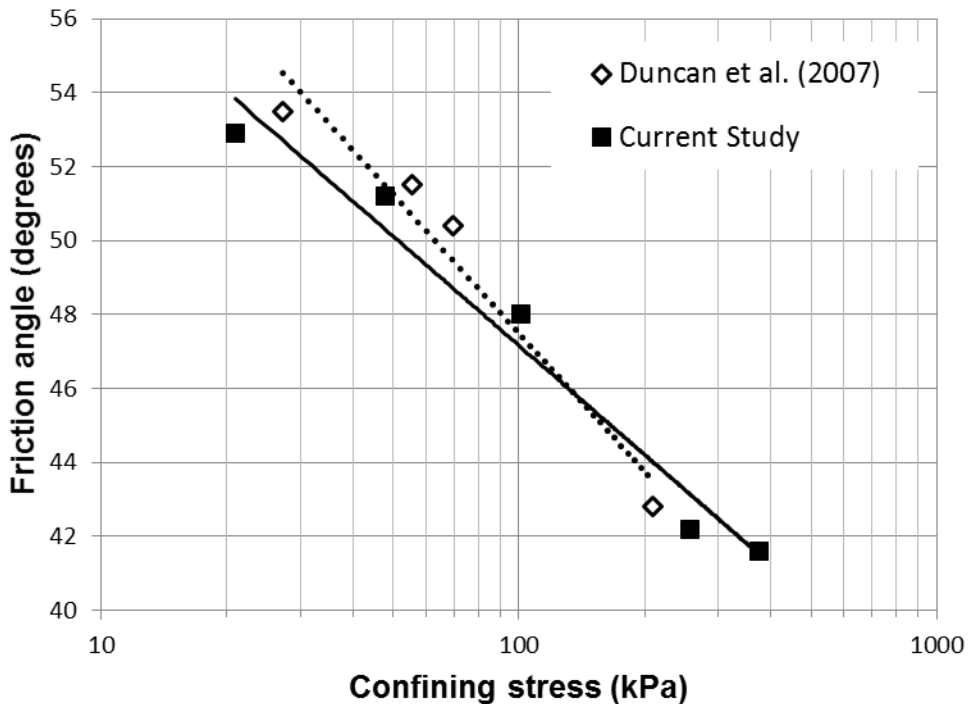


Figure 5.20 Friction angle versus confining stress for the aggregate used in this study and the #57 limestone from Duncan et al. (2007)

5.5 Summary of Results

This chapter summarized the geotechnical characterization and mechanical behavior of limestone aggregate. Comparison of the stress-strain and volumetric strain behavior of the tests from this study to the previous work of Duncan et al. (2007) were made between tests with similar confining pressure.

The aggregate had particle sizes ranging from less than 7.5 μm to 22.4 mm. The aggregate was classified as a poorly-graded gravel (GP), with a specific gravity of 2.701. The minimum and maximum void ratios were calculated to be 0.44 and 1.01, respectively. The stress-strain relationships exhibited strain softening behavior for each of the tests, incurring axial strains at failure between 4.1 and 11.3 percent. The principal

stress difference at failure occurred at higher corresponding axial strains for higher confining pressures, indicating that specimens with a higher confining pressure were able to sustain larger axial strains before reaching failure. Volumetric strain behavior was modeled and four of the five tests exhibited dilatant behavior with varying levels of volume change. Only the highest confining pressure, with an effective confining stress of 357 kPa, was high enough to prevent dilation. The specimen sheared at 357 kPa demonstrated continuous compression with no dilatant behavior. The peak and residual friction angles for each of the tests were calculated and they ranged from 52.9 to 41.6 and 49.1 to 40.8, respectively.

Hyperbolic models were fit to the data according to Duncan et al. (1980). For the tests at lower confining stresses, up to 101 kPa, the hyperbolic curve closely modeled the actual curve up to approximately 3.5 percent axial strain. For the specimen sheared at 257 kPa the hyperbolic curve was accurate up to approximately 6.0 percent axial strain, and for the specimen sheared at 375 kPa the hyperbolic curve demonstrated close agreement with the actual curve up to approximately 8.5 percent axial strain.

Lastly, the stress-strain and volumetric strain behavior was compared to tests done on a similar aggregate by Duncan et al. (2007). The comparison of the stress-strain and strain-strain relationships and the friction angles of these two determined that similar aggregates with small differences in gradation, composition, and with relative densities between 66 and 95 percent exhibit similar mechanical properties.

6.0 Summary, Conclusions, and Suggestions for Further Study

6.1 Summary of Research Performed

This study determined the geotechnical characterization and drained shear strength of a limestone aggregate commonly used for the construction of aggregate piers. The index properties of the specific gradation were found including minimum and maximum void ratios, specific gravity and the Modified Proctor compaction characteristics. The drained shear strength parameters were found using consolidated drained, axisymmetric triaxial testing. Five confining stresses were chosen to model the stresses an aggregate pier would be subjected to in situ and at a given depth. The five tests were performed at 21, 48, 101, 257, and 375 kPa effective confining stresses, respectively. The post-consolidation relative density ranged from 66 to 86 percent. This information will be useful for those performing numerical analyses of aggregate pier reinforced soils.

6.2 Conclusions

Inspection of the results of the index testing and consolidated drained triaxial testing indicates that:

- The limestone aggregate was a poorly graded gravel, and had a specific gravity of 2.701;
- The minimum and maximum void ratios were determined to be 0.44 and 1.01, respectively;

- The specimens demonstrated strain softening behavior without a distinctive peak and a gradual decrease in principal stress difference after failure;
- The axial strain at failure ranged from 4.1 to 11.3 percent, increasing with increasing confining stress;
- Dilation occurred at most of the confining stresses but decreased in magnitude with increased confining stresses until no dilative behavior with the highest confining stress (i.e., 375 kPa);
- The peak and residual friction angles ranged from 52.9 to 41.6 degrees and 49.1 to 40.8 degrees, respectively. The friction angle decreased with increases in confining pressure. Small differences were observed between the peak and residual friction angles, with the difference decreasing at higher confining pressures;
- The friction angle did not vary significantly within a large range of relative densities because other factors such as angularity have a much greater impact than density for these aggregates;
- Hyperbolic models were fitted to the data using the Duncan-Chang model described by Duncan et al. (1980). The hyperbolic curves closely modeled the actual behavior up to approximately 3.5 percent axial strain for the 21, 48, and 101 kPa confining stresses, up to approximately 6.0 percent axial strain for the 257 kPa confining stress, and up to approximately 8.5 percent axial strain for the specimen sheared at 375 kPa;

- The stress-strain, volumetric strain behavior and friction angles determined for the tests in this study were comparable to the friction angles and behavior modeled for the #57 limestone aggregate from Duncan et al. (2007).

6.3 Suggestions for Further Study

The understanding of the bearing failure mechanism of aggregate piers remains largely unstudied. The effects of design variables on the failure mechanisms are not fully understood. But as an economically viable means of ground improvement, research on aggregate piers is vital for advancing the technique. Future experimental research could include:

- Evaluating the effect of cement content on the strength of an aggregate;
- Performing additional tests on aggregates with different angularities, but similar gradations to better understand the effect of angularity on the strength of a material;
- Performing additional tests on this aggregate with a different gradation to better understand the effect of gradation on the strength of a material;
- Evaluating the correlation between the strength parameters of the aggregate determined in the laboratory and the behavior of an aggregate pier in situ.

References

- ASTM (2006a). "Standard Test Methods for Maximum Index Density and Unit Weight of Soils Using a Vibratory Table." *D 4253-00 (Reapproved 2006)*, ASTM International, West Conshohocken, PA.
- ASTM (2006b). "Standard Test Methods for Minimum Index Density and Unit Weight of Soils and Calculation of Relative Density." *D 4254-00 (Reapproved 2006)*, ASTM International, West Conshohocken, PA.
- ASTM (2007). "Standard Practice for Correction of Unit Weight and Water Content for Soils Containing Oversize Particles." *D 4718-87 (Reapproved 2007)*, ASTM International, West Conshohocken, PA.
- ASTM (2011). "Standard Practice for Classification of Soils for Engineering Purposes (Unified Soil Classification System)." *D 2487-11*, ASTM International, West Conshohocken, PA.
- ASTM (2012). "Standard Test Methods for Laboratory Compaction Characteristics of Soil Using Modified Effort (56,000 ft-lbf/ft³ (2,700 kN-m/m³))." *D 1557-12*, ASTM International, West Conshohocken, PA.
- Duncan, J. M., Brandon, T., Jian, W., Smith, G., Park, Y., Griffith, T., Corton, J., and Ryan, E. (2007). "Densities and Friction Angles of Granular Materials with Standard Gradations 21b and #57." *Rep. CGPR #45*, Center for Geotechnical Practice and Research, Virginia Polytechnic Institute, Blacksburg, VA.
- Duncan, J. M., Byrne, P., Wong, K. S., and Mabry, P. (1980). "STRENGTH, STRESS-STRAIN AND BULK MODULUS PARAMETERS FOR FINITE ELEMENT ANALYSES OF STRESSES AND MOVEMENTS IN SOIL MASSES." *Rep. UCB/GT/80-01*, College of Engineering, Office of Research Services, University of California-Berkeley, Berkeley, CA.
- Duncan, J. M. and Chang, C. Y., "Nonlinear analysis of stress and strain in soils", *Journal of the Soil Mechanics and Foundations Division*, ASCE, 96(SM5), 1629-1653, 1970.
- Hayward Baker. (2012a). "Vibro Piers (Aggregate Piers)." <<http://haywardbaker.com/WhatWeDo/Techniques/GroundImprovement/VibroPiers/default.aspx>>. (October, 2014).
- Hayward Baker. (2012b). "Vibro Replacement (Stone Columns)." <<http://haywardbaker.com/WhatWeDo/Techniques/GroundImprovement/VibroReplacement/default.aspx>>. (October, 2014).

- Holtz, R. D., Kovacs, W. D., and Sheahan, T. C. (2011). *An Introduction To Geotechnical Engineering*, Pearson Education, Inc., Upper Saddle River, NJ.
- Lee, K. L. (1965). "Triaxial Compressive Strength of Saturated Sands Under Seismic Loading Conditions." Ph.D. dissertation, University of California, Berkeley.
- Stuedlein, A. W. (2008). "Bearing capacity and displacement of spread footings on aggregate pier reinforced clay." Ph.D thesis, University of Washington, Seattle.
- Stuedlein, A. W., and Holtz, R. D. (2012). "Analysis of Footing Load Tests on Aggregate Pier Reinforced Clay." *Journal of Geotechnical and Geoenvironmental Engineering*, 138(9), pp. 1091-1103.
- Youd, T. L. (1973). "Factors Controlling Maximum and Minimum Densities of Sands." *Evaluation of Relative Density and Its Role in Geotechnical Projects Involving Cohesionless Soils, ASTM STP 523*, American Society for Testing and Materials, pp. 98-112.

Appendix A: Stress-Strain and Volumetric Strain Curves for Individual Tests

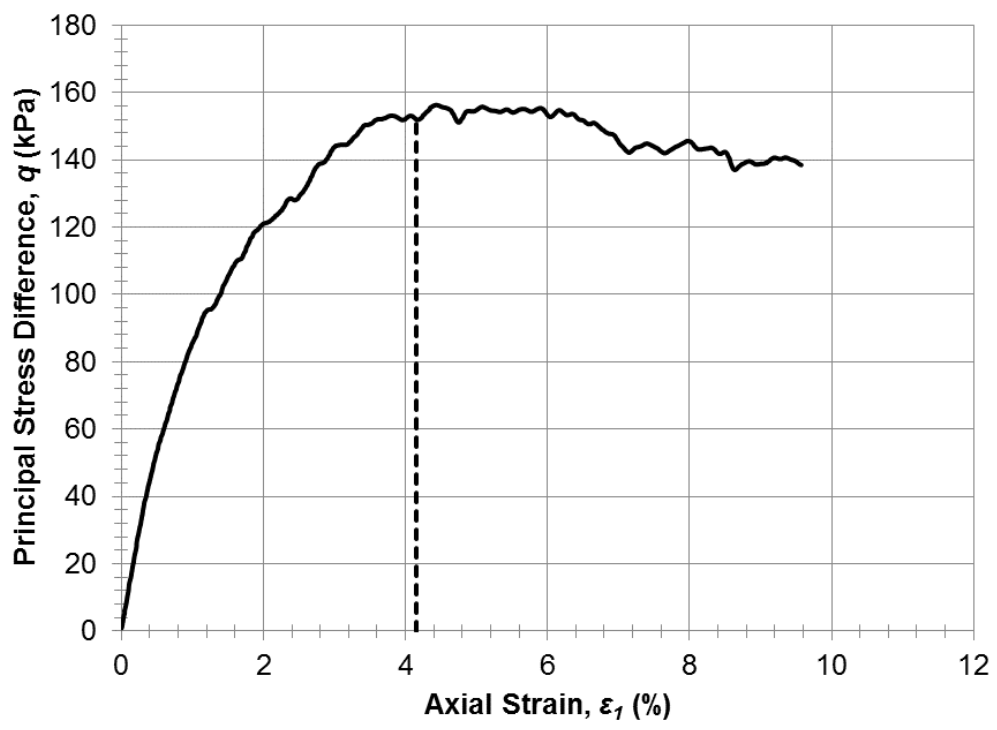


Figure A.1 Principal stress difference versus axial strain for specimen sheared at 21 kPa effective confining stress, dashed line indicates strain at failure

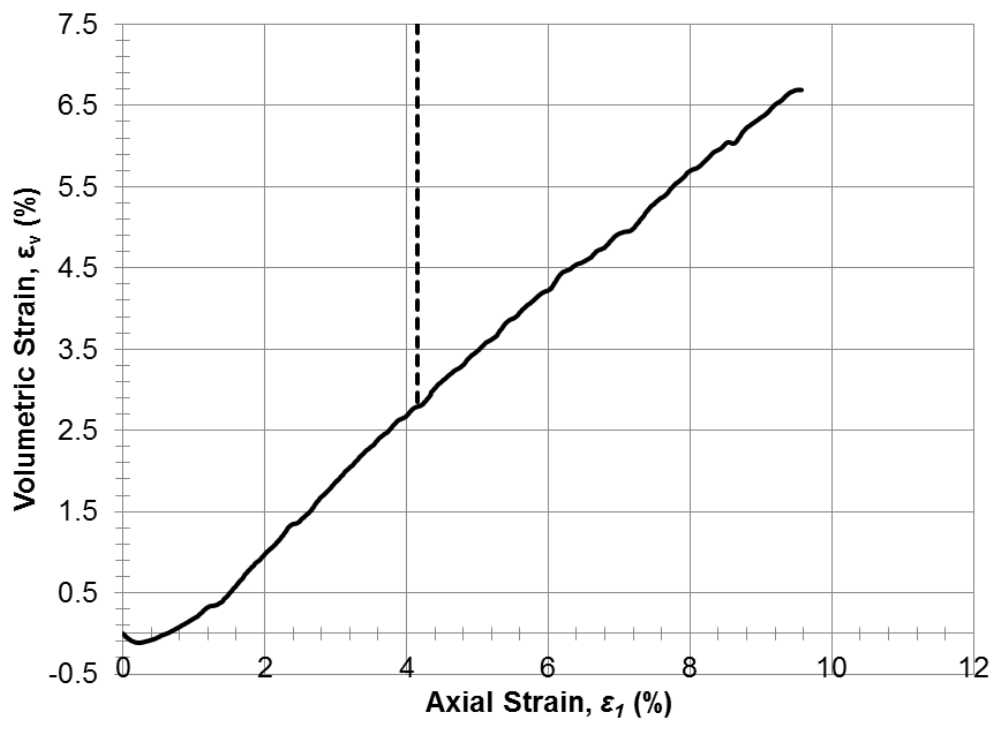


Figure A.2 Volumetric strain versus axial strain for specimen sheared at 21 kPa effective confining stress, dashed line indicates strain at failure

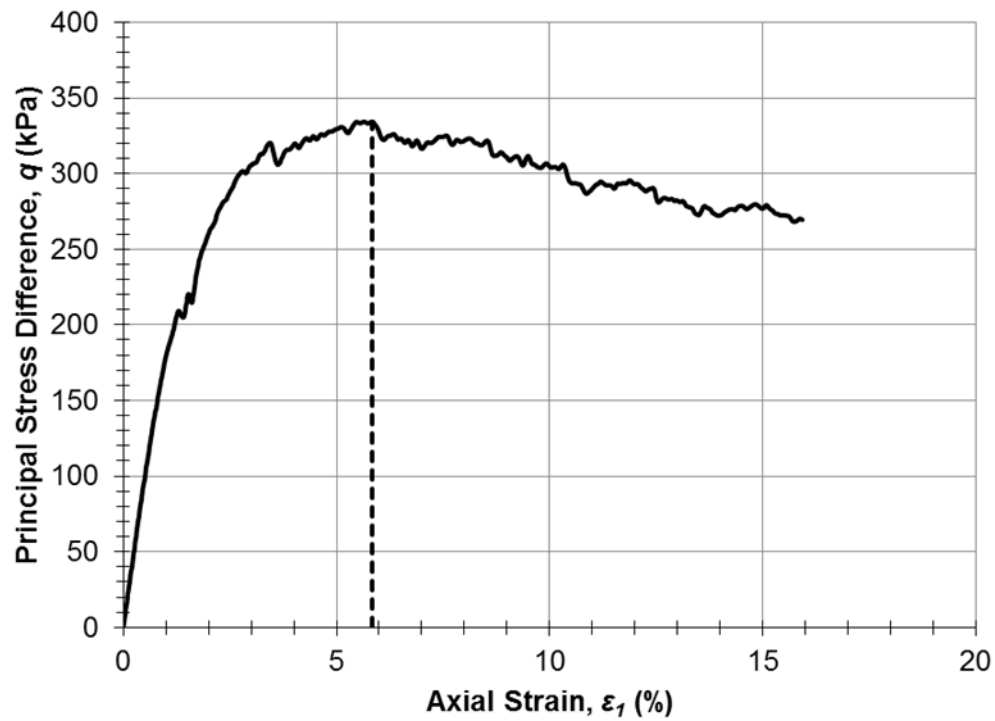


Figure A.3 Principal stress difference versus axial strain for specimen sheared at 48 kPa effective confining stress, dashed line indicates strain at failure

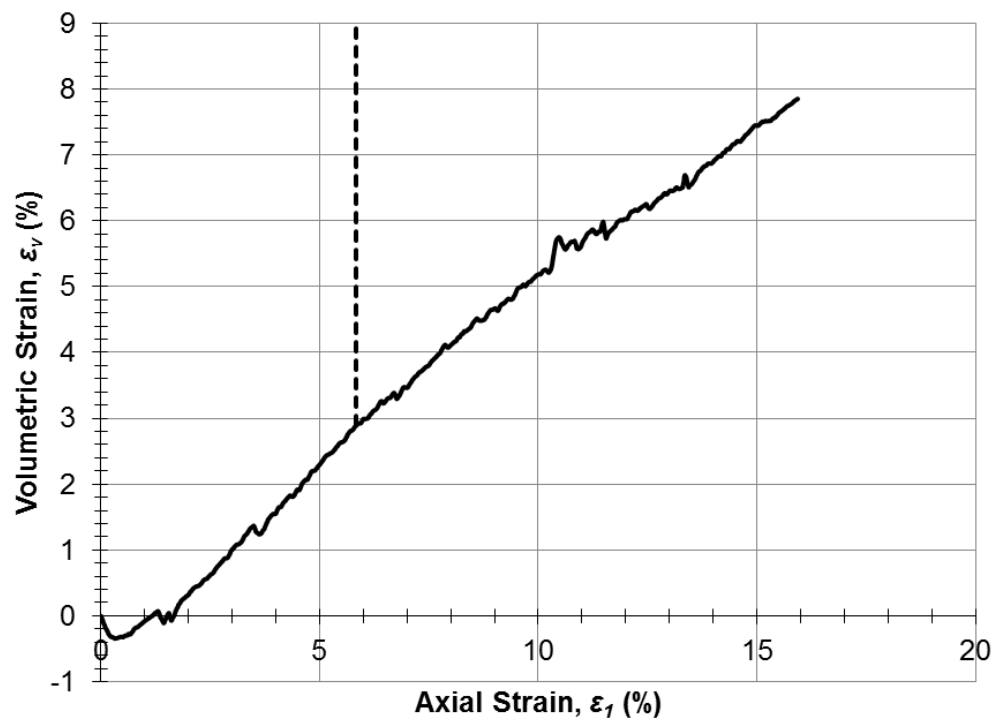


Figure A.4 Volumetric strain versus axial strain for specimen sheared at 48 kPa effective confining stress, dashed line indicates strain at failure

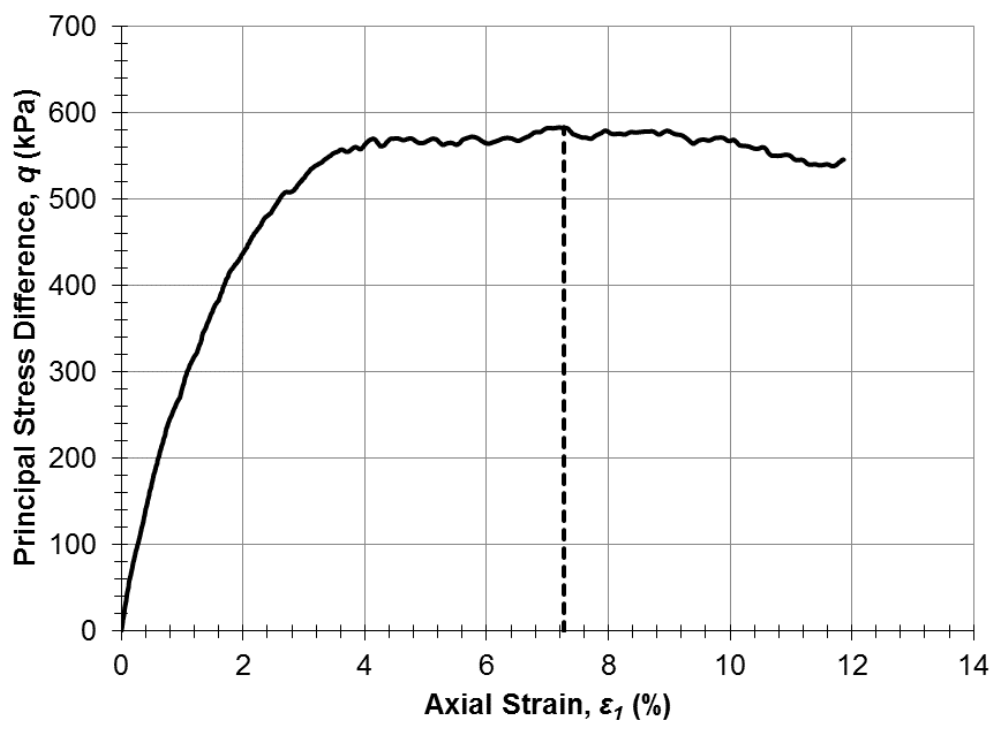


Figure A.5 Principal stress difference versus axial strain for specimen sheared at 101 kPa effective confining stress, dashed line indicates strain at failure

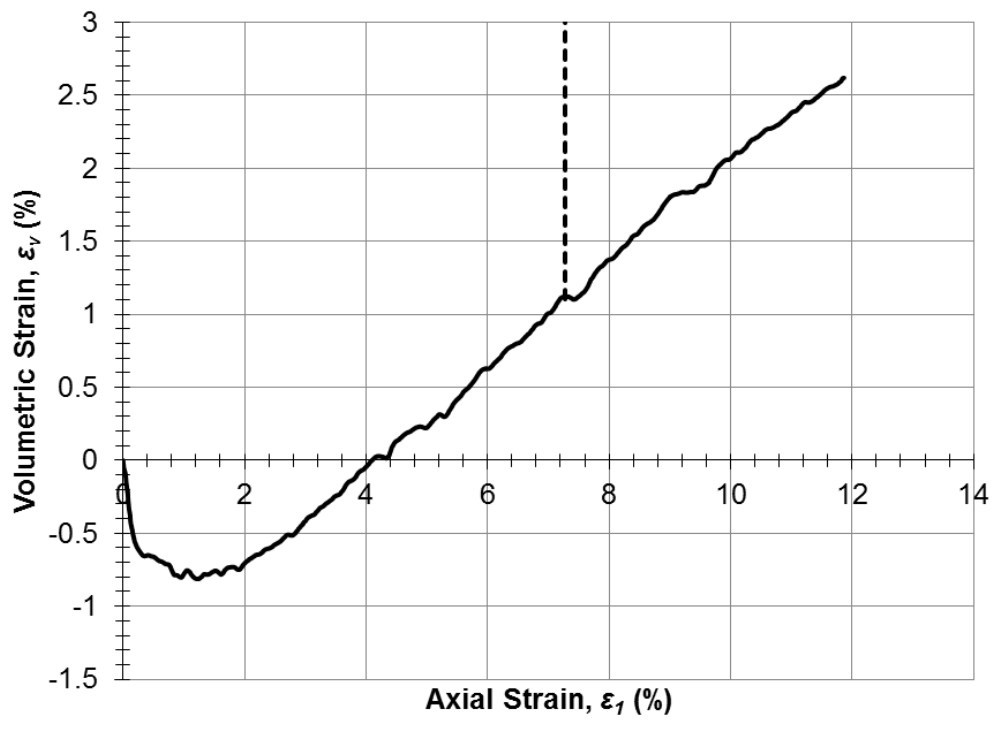


Figure A.6 Volumetric strain versus axial strain for specimen sheared at 101 kPa effective confining stress, dashed line indicates strain at failure

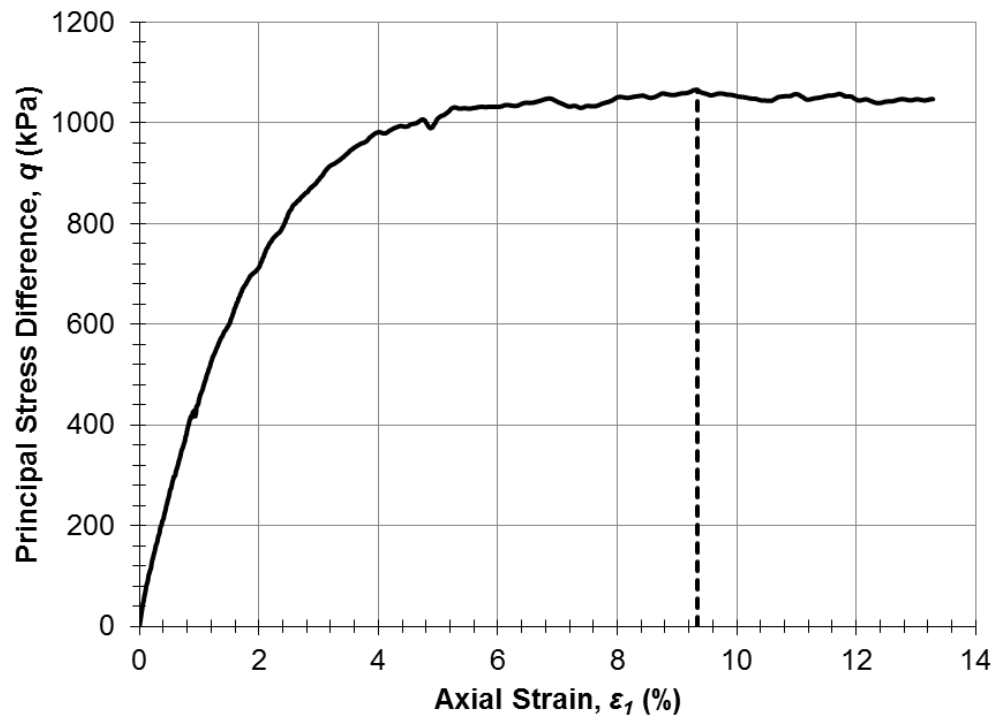


Figure A.7 Principal stress difference versus axial strain for specimen sheared at 257 kPa effective confining stress, dashed line indicates strain at failure

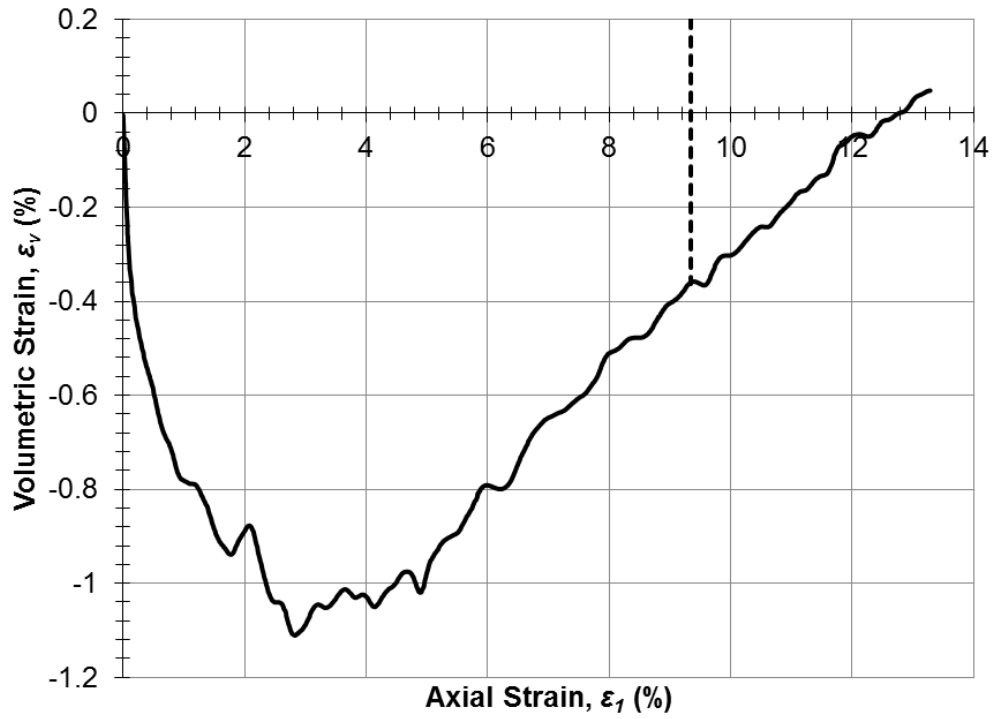


Figure A.8 Volumetric strain versus axial strain for specimen sheared at 257 kPa effective confining stress, dashed line indicates strain at failure

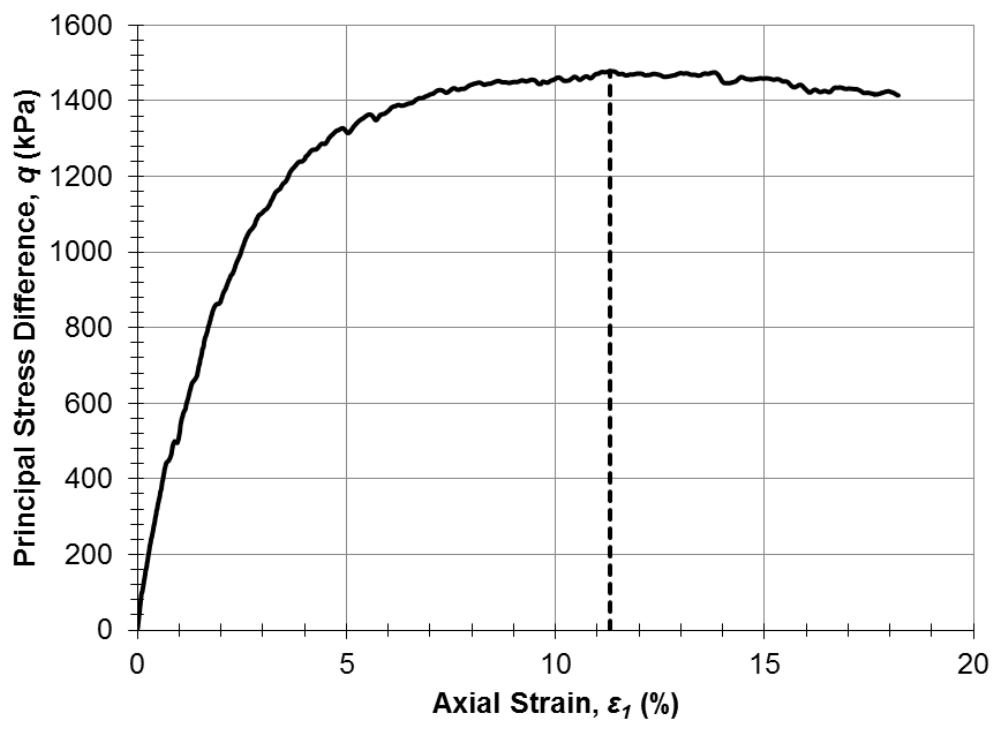


Figure A.9 Principal stress difference versus axial strain for specimen sheared at 375 kPa effective confining stress, dashed line indicates strain at failure

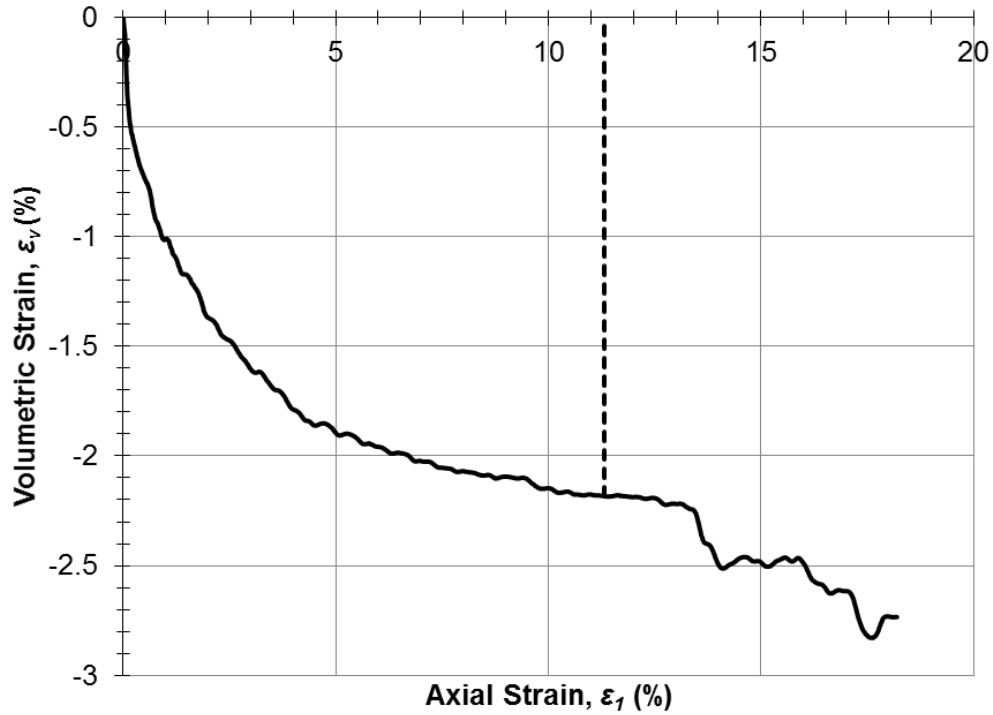


Figure A.10 Volumetric strain versus axial strain for specimen sheared at 375 kPa effective confining stress, dashed line indicates strain at failure

Appendix B: Data used for Hyperbolic Stress-Strain Curves

Table B.1 Data used for Hyperbolic Stress-Strain Curves

| σ'_3 (kPa) | q_f (kPa) | $\varepsilon_{1,70\%}$ (%) | $q_{70\%}$ (kPa) | $(\varepsilon_1/q)_{70\%}$ (kPa ⁻¹) | $\varepsilon_{1,95\%}$ (%) | $q_{95\%}$ (kPa) | $(\varepsilon_1/q)_{95\%}$ (kPa ⁻¹) | $1/q_{ult}$ (kPa ⁻¹) | E_i/P_a |
|----------------------|----------------|-------------------------------|---------------------|--|-------------------------------|---------------------|--|-------------------------------------|-----------|
| 21 | 152 | 1.53 | 106 | 1.44e-04 | 3.06 | 144 | 2.12e-04 | 4.44e-05 | 130 |
| 48 | 334 | 1.71 | 234 | 7.33e-05 | 3.35 | 317 | 1.06e-04 | 1.99e-05 | 252 |
| 101 | 582 | 1.72 | 407 | 4.23e-05 | 3.49 | 553 | 6.30e-05 | 1.17e-05 | 449 |
| 357 | 1096 | 2.14 | 767 | 2.79e-05 | 5.09 | 1041 | 4.89e-05 | 7.12e-06 | 779 |
| 375 | 1478 | 2.59 | 1035 | 2.50e-05 | 6.69 | 1404 | 4.77e-05 | 5.54e-06 | 926 |

